SDR enzymes oxidize specific lipidic alkynylcarbinols into cytotoxic protein-reactive species

Pascal Demange[1,¤], Etienne Joly[1,¤], Julien Marcoux[1,¤], Patrick R. A. Zanon[2], Dymytrii Listunov[3,4], Pauline Rullière[3], Cécile Barthes[4], Céline Noirot[5], Jean-Baptiste Izquierdo[1], Karen Pradines[1,6], Romain Hee[1,6], Maria Vieira de Brito[4,7], Marlène Marcellin[1], Rémi-Félix Serre[8], Olivier Bouchez[8], Odile Burlet-Schiltz[1], Maria Conceição Ferreira Oliveira[7], Stéphanie Ballereau[3], Vania Bernardes-Génisson[4], Valérie Maraval[4], Patrick Calsou[1,2], Stephan M. Hacker[2], Yves Génisson[3,†,*], Remi Chauvin[4,†,*], Sébastien Britton[1,6,*]

* corresponding authors. ¤, † equal contribution.

AFFILIATIONS:

1 Institut de Pharmacologie et de Biologie Structurale, IPBS, Université de Toulouse, CNRS, UPS, Toulouse, France.

2 Department of Chemistry, Technical University of Munich, Lichtenbergstrasse 4, 85748 Garching, Germany

3 LSPCMIB, UMR5068, CNRS, Université de Toulouse, UPS, 118 route de Narbonne, 31062 Toulouse, France.

4 LCC-CNRS, Université de Toulouse, CNRS, UPS, Toulouse, France.

5 INRAE, UR 875 Unité de Mathématique et Informatique Appliquées, Genotoul Bioinfo, Auzeville, CS 52627, 31326, Castanet-Tolosan, France.

6 Equipe labellisée la Ligue contre le Cancer 2018.

7 Department of Organic and Inorganic Chemistry, Science Center, Federal University of Ceará, Fortaleza-CE, 60455-970, Brazil.

8 INRAE, US 1426 GeT-PlaGe, F-31326, Castanet-Tolosan, France.

ABSTRACT:

Hundreds of cytotoxic natural or synthetic lipidic compounds contain chiral alkynylcarbinol motifs, but the mechanism of action of those potential therapeutic agents remains unknown. Using a genetic screen in haploid human cells, we discovered that the enantiospecific cytotoxicity of numerous terminal alkynylcarbinols, including the highly cytotoxic dialkynylcarbinols, involves a bioactivation by HSD17B11, a short-chain dehydrogenase/reductase (SDR) known to oxidize the C-17 carbinol center of androstan-3-alpha,17-beta-diol to the corresponding ketone. A similar oxidation of dialkynylcarbinols generates dialkynylketones, that we characterize as highly protein-reactive electrophiles. We established that, once bioactivated in cells, the dialkynylcarbinols covalently modify several proteins involved in protein-quality control mechanisms, resulting in their lipoxidation on cysteines and lysines through *Michael* addition. For some proteins, this triggers their association to cellular membranes and results in endoplasmic reticulum stress, unfolded protein response activation, ubiquitin-proteasome system inhibition and cell death by apoptosis. Finally, as a proof-of-concept, we show that generic lipidic alkynylcarbinols can be devised to be bioactivated by other SDRs, including human RDH11 and HPGD/15-PGDH. Given that the SDR superfamily is one of the largest and most ubiquitous, this unique cytotoxic mechanism-of-action could be widely exploited to treat diseases, in particular cancer, through the design of tailored prodrugs.

MAIN TEXT

Introduction

Nature is a rich source of bioactive compounds, some of which can be directly exploited to treat diseases. Some of them reveal sophisticated mechanisms of action which can be mimicked by designing synthetic molecules with specific features (1). Marine sponges have attracted pharmaceutical interest since the discovery in the 1950s of C-nucleosides in *Cryptotethia crypta* that led to the development of cytosine arabinoside (ara-C or cytarabine) and analogues as anticancer treatments for acute myelogenous leukemia (2,3). In a different structural series, several cytotoxic acetylenic lipids bearing a terminal alkenylalkynylcarbinol (AAC) pharmacophore have since been isolated from marine sponges, such as petrocortyne A (**Supplementary Figure 1**), isolated from *Petrosia sp*. (4) and fulvinol isolated from *Haliclona fulva* (5). The simplest cytotoxic AAC representative, (*S*)-eicos-(*4E*)-en-1-yn-3-ol ((*S*)-**1**, **Supplementary Figure 1**), was isolated from the marine sponge *Cribrochalina vasculum* (6). It demonstrated high cytotoxic activity selectively towards non-small cell lung carcinoma cells as compared to normal lung fibroblasts (7). Starting from (*S*)-**1**, an extensive structure-activity relationship study in human cancer cell lines established that (**Supplementary Figure 1**): i) the non-natural enantiomer (*R*)-**1** has higher cytotoxic activity, ii) homologues with shorter lipidic tails are more cytotoxic, with an optimum total aliphatic backbone of 17 carbon atoms (e.g. (*R*)-**2**), and iii) replacement of the internal C=C bond by a C≡C bond, giving rise to a terminal dialkynylcarbinol (DAC) pharmacophore, further increases cytotoxicity, to reach an IC_{50} down to 90 nM for the DAC (*S*)-**3** (8-10). However, despite this significant level of activity, the mode of action of this family of molecules, including the natural compound (*S*)-**1**, remains elusive (7).

Here we use functional genomics and chemoproteomics to decipher how cytotoxic DACs and related molecules mediate their biological effect. We discover that they behave as prodrugs enantiospecifically bioactivated by a member of the Short-chain Dehydrogenase/Reductase

(SDR) family. Finally, we design new SDR-bioactivated DACs derivatives, establishing this family of lipidic alkynylcarbinols as a large and untapped reservoir of cytotoxic prodrugs.

Results

The SDR HSD17B11 governs (*S*)-DACs cytotoxicity. To determine how cytotoxic DACs mediate their effect on human cells, we applied a genetic approach using the pseudo-haploid human cell line HAP-1 (11). Given that (*S*)-**3** had the greatest cytotoxic activity of all the DACs previously tested (8-10), we screened for mutations that could render HAP-1 cells resistant to (*S*)-**3.** We first confirmed in HAP-1 that (*S*)-**3**, but not (*R*)-**3** (**Figure 1A**), exhibits nanomolar cytotoxic activity (**Figure 1B**, IC_{50} 62.4 nM), in agreement with previous results on HCT116 colon cancer cells (8). We used Ethyl-Methane Sulfonate (EMS) to generate a mutagenized HAP-1 population and selected resistant clones using a lethal 250 nM (*S*)-**3** concentration. Ten individual (*S*)-**3**-resistant clones (DACR) were isolated, displaying a 38- to 62-fold resistance to (*S*)-**3** (**Figure 1C**) but similar sensitivity as parental cells to two unrelated compounds, bortezomib and doxorubicin (**Supplementary Figure 2A,B**). Based on previous work (12,13), and considering that EMS induces mainly point mutations under these conditions (14), we selected four DACR clones for RNA-seq analysis, to identify mis- or non-sense mutations accounting for the resistance. Around nine mutated genes were identified per clone (**Supplementary Figure 2C**), with *KCTD5* and *HSD17B11* being the only mutated genes shared by more than two clones (**Supplementary Figure 2D**). *KCTD5* encodes for an E3-ubiquitin ligase substrate adaptor identified in a genetic screen as a negative regulator of the Akt pathway (15). However, while *KCTD5* mRNA was expressed in all DACR clones, *HSD17B11* mRNA levels were strongly reduced in the only clone without *HSD17B11* coding mutations (#A5, **Supplementary Figure 2E**). This suggested that mutations or lack of expression of *HSD17B11* were responsible for DACR clone resistance. To confirm this, we sequenced *HSD17B11* cDNAs from six other DACR clones, and detected non-

synonymous *HSD17B11* mutations in five, and no *HSD17B11* cDNA in the sixth, suggesting loss of expression (**Figure 1D,E**). These data strongly supported a role for *HSD17B11* in mediating (*S*)-**3** cytotoxicity.

HSD17B11 encodes for the estradiol 17-beta-dehydrogenase 11, a member of the SDR super-family. HSD17B11, also called SDR16C2, PAN1B, DHRS8 or retSDR2, localizes to the endoplasmic reticulum (ER) and lipid droplets (LD) via a N-terminal targeting domain (**Figure 1E**), where it uses NAD+ to catalyze oxidation of the C17 carbinol center of androstan-3-alpha,17-beta-diol to generate androsterone (16,17) (see **Figure 2A**). The HSD17B11 protein was barely detectable in all the DACR clones (**Figure 1F**, lower band), suggesting that the mutations result in protein instability. Using the DACR#A5 clone, in which *HSD17B11* RNA was strongly down-regulated (~200 fold, **Supplementary Figure 2E**), we performed complementation experiments with plasmids coding for GFP alone, or wild-type (WT) or S172L HSD17B11-GFP. This mutation was selected because the S172 residue is critical for catalysis (18), and the DACR#A4 clone, which carried S172L mutations, was the only one in which traces of full length HSD17B11 could be detected (**Figure 1F**). Complemented DACR#A5 cells stably expressing WT and S172L HSD17B11-GFP at similar levels were successfully isolated (**Figure 1G**), and (*S*)-**3** was ~50 times more active against cells expressing WT HSD17B11 compared to control GFP-complemented cells or cells expressing S172L HSD17B11 (**Figure 1H**). This supports that HSD17B11 catalytic activity is critical for (*S*)-DAC cytotoxicity. Notably, the DACR#A4 clone (S172L mutation) was also resistant to six other cytotoxic AACs: the naturally occurring AAC (*S*)-**1** (**Supplementary Figure 3A**), its synthetic enantiomer (*R*)-**1**, its shorter homologue (*R*)-**2**, the synthetic AAC (*S*)-**4** with an internal C≡C bond and an external C=C bond (**Supplementary Figure 3B**), the allenylalkynylcarbinol (AllAC) (*R*,S_a)-**5** (19) and the more cytotoxic butadiynylalkynylcarbinol (BAC) (*S*)-**6** (20) (**Supplementary Figure 3C**). Thus, HSD17B11 functionality governs the enantiospecific cytotoxicity of the natural compound (*S*)-**1** but also of all the more cytotoxic

synthetic derivatives tested. In addition, HSD17B11 has been recently identified as mediating, through an unknown mechanism, the cytotoxic effect of dehydrofalcarinol, a polyacetylenic compound with a terminal butadiynylalkenylcarbinol motif isolated from several plants of the *Asteraceae* family (21).

We next tested the cytotoxic activity of (*S*)-**3** on a panel of 15 cancer cell lines. This revealed that the osteosarcoma U2OS cell line was the most sensitive to (*S*)-**3** while the breast cancer cell line T47D was highly resistant (**Supplementary Figure 4A**). In agreement, HSD17B11 protein was undetectable in T47D, while U2OS displayed the highest levels (**Supplementary Figure 4B**), in agreement with reported mRNA levels (*The Cancer Cell Line Encyclopedia dataset* (22)). In addition, (*S*)-**3** was particularly cytotoxic toward four other osteosarcoma cell lines as compared to normal cell lines or primary osteoblasts (**Supplementary Figure 4C**), suggesting that DACs could prove useful to treat this type of cancer. CRISPR/Cas9-mediated inactivation of HSD17B11 also conferred significant (*S*)-**3** resistance to U2OS cells, which was suppressed by wild-type HSD17B11-GFP but not by the S172L mutant or GFP alone (**Supplementary Figure 5A,B**). This was further confirmed using two different small-interfering RNAs (siRNA) to down-regulate HSD17B11 in U2OS (**Supplementary Figure 5C,D**) and in the non-small cell lung carcinoma cell line A549, in which CRISPR/Cas9-mediated HSD17B11 inactivation also conferred (*S*)-**3** resistance (**Supplementary Figure 5E,F**). Altogether, these data establish that HSD17B11 is critical in multiple cell lines for (*S*)-**3** cytotoxic activity, and suggest that (*S*)-**3** behaves as an HSD17B11-bioactivated prodrug. In addition, the acute toxicity of (*S*)-**3** towards osteosarcoma cell lines indicates that DACs could be developed into a targeted anti-cancer therapy.

Dialkynylketones are protein-reactive species. We next investigated the downstream mechanism of cytotoxic action of the DAC (*S*)-**3.** The C17 carbinol center of androstan-3-alpha,17-beta-diol, which is naturally oxidized by HSD17B11 (**Figure 2A** (16)), has the same spatial orientation as the (*S*)-**3** carbinol when its lipidic chain is superimposed with the C13(C18) side of

the steroid skeleton (**Figure 2B**). This suggested that HSD17B11 enantiospecifically recognizes and oxidizes (*S*)-**3** into a "dialkynylketone" **7** (DACone), a diynone that could be the cytotoxic species. However, when the DACone **7** was previously synthesized and tested, no cytotoxic activity was found (9). Given the high *in vitro* electrophilic reactivity of ynones as *Michael* acceptors of thiols and amines (23), we considered that medium components such as serum albumin may rapidly react with and inactivate DACones. To test this, we synthesized the DACone **7**, as well as a homologue with a shorter alkyl chain **8,** and treated U2OS cells in a protein-free medium (PBS containing $CaCl_2$ and $MgCl_2$ to maintain cellular adhesion). Both the DACones **7** and **8** were indeed cytotoxic in the absence of serum, with **8** (short chain) being even more active than (*S*)-**3** (**Figure 2C**). While the cytotoxicity of (*S*)-**3** was strongly reduced by inactivation of HSD17B11, the cytotoxicity of the DACones **7** and **8** was not affected, supporting the notion that the DACones are the cytotoxic products generated from DACs by HSD17B11.

To further analyze the interaction between DACones and proteins, we used copper-mediated azide-alkyne cycloaddition (CuAAC "click chemistry"), which can be used to monitor what happens to drugs in various biological environments, including inside cells (24,25). We synthesized "clickable" analogues, i.e. bearing a terminal C≡CH tag, for each DAC enantiomer ((*S*)-**9** and (*R*)-**9**), and for long and short DACones (**10** and **11**, **Figure 2B**), and used them to monitor the formation of covalent bonds between DACones and serum proteins. The clickable DACone **10**, or clickable DAC (*S*)-**9** as control, were incubated with fetal bovine serum (FBS) or purified bovine serum albumin (BSA), followed by CuAAC-mediated ligation of an AlexaFluor647-azido fluorophore to the free C≡CH tag. The proteins were separated by SDS-PAGE and scanned for fluorescence (26). Covalent adducts were formed on BSA with DACone **10** but not with (*S*)-**9** (**Figure 2D**). Moreover, the DACone **10** also reacted with several other model proteins, including the bovine beta-lactoglobuline (BLG) (**Supplementary Figure 6A**). Using BSA and BLG, we established that DACone adducts are produced only when using the clickable DACones **10** or **11**

(**Figure 2E**), suggesting that the terminal triple bond of the DACone pharmacophore is modified or masked after reaction. Finally, we could recapitulate the activation of (*S*)-**9**, but not of (*R*)-**9**, into protein-reactive species by immunopurified WT HSD17B11, but not by the S172L mutant (**Figure 2F**). This further supports an enantio-selective bioactivation of (*S*)-**9** into the DACone **10** by HSD17B11.

Reaction of DACones with proteins. To further decipher the reaction of DACones with proteins, we used direct-infusion mass spectrometry to analyze BLG modified with the clickable DACone **10**. Purified BLG contains two isoforms (A and B, differing by 86.0 Da) and, when incubated in a 1:3 molar ratio with DACone, both BLG isoforms were completely modified with the formation of one or two adducts of ~+242 Da (**Figure 2G**), which corresponds to the mass of the clickable DACone **10**. Monitoring the absorbance spectra of modified BLG revealed that BLG gains an absorption band at ~323 nm upon modification by DACone (**Supplementary Figure 6B**). Using this, we confirmed that both BLG and BSA are modified by the DACones **7** and **8** or their clickable analogues **10** and **11** (**Supplementary Figure 6B,C**). The shorter DACone **8** proved even more reactive, in line with its greater cytotoxicity (**Figure 2C**, **Supplementary Figure 6B,C**). Next, we assessed the selectivity of DACones towards amino acid residues in the whole proteome in an unbiased fashion. For this purpose, we incubated the DACones **10** and **11** with U2OS total cell extracts in PBS. We then used residue-specific chemoproteomics with isotopically labelled desthiobiotin azide (isoDTB) tags (27-29) coupled to a novel MSFragger-based FragPipe computational platform (30) to detect the modified amino acids on the enriched peptides. This revealed that both DACones reacted with cysteine and lysine side chains, with the expected modification being detected (**Figure 2H, Supplementary Figure 6D,E,F, Supplementary File 1**). As we also detected many unmodified peptides, we cannot exclude that other amino acids are also modified by the probe but that their modification is lost during the workflow. We next confirmed the reactivity of DACones with cysteine and lysine side chains by monitoring the appearance of

the ~323 nm absorbance band after reaction of the DACone **8** with isolated amino acids, using *N*-acetylated versions to prevent reactions with the N-terminal amino group. At neutral pH, DACones only reacted with *N*-acetyl-L-cysteine (NAC) but not with N_α-acetyl-L-lysine (NAK) (**Supplementary Figure 6G**, left spectrum), whereas at higher pH they reacted with both NAC and NAK (**Supplementary Figure 6G**, right spectrum), in agreement with the nucleophilic reactivity of the non-protonated ε–NH_2 group of the lysine chain. No reaction was observed with *N*-acetyl glycine (NAG), supporting that the reaction involves the side chain. The reaction with lysine side chains is compatible with the pK_a value for the lysine ε-amino group that can be as low as ~5 in hydrophobic domains in proteins (31). In agreement, analysis of the sequence context of the amino acids identified as modified by the DACone **10** revealed an enrichment of hydrophobic amino acids around the modified lysines, which was not observed for the modified cysteines (**Supplementary Figure 7A,B, Supplementary File 2**). Using nuclear magnetic resonance (NMR), we characterized the products of the reaction of the short DACone **8** with NAC (**Supplementary Figure 8A,B**) or NAK (**Supplementary Figure 8C,D**). This revealed that a covalent bond forms by addition of the thiol (NAC) or amino (NAK) group onto the terminal alkyne of the DACone head (**Supplementary Figure 8E**) and suggests a similar reaction with proteins (**Figure 2I**). The donor-acceptor extension of π-electron delocalization in the enone adducts (S–CH=CH–C=O for NAC, N–CH=CH–C=O for NAK) accounts for the additional absorption band observed for the DACone adducts with *N*-acetyl amino acids. Altogether, our data show that DACones are highly reactive with proteins *in vitro*.

Bioactivated (*S*)-DACs lipoxidize multiple proteins in cells. Protein modification by lipidic DACs equates to their lipoxidation (a term used to designate the covalent modification of a protein by a reactive lipid (32)) by one or several C17 hydrophobic chain(s). Considering that protein palmitoylation (addition of a C16 lipidic chain) can trigger membrane tethering of proteins, we hypothesized that lipoxidation by DACs could affect protein localization and/or function and

account for the cytotoxicity of bioactivated DACs in cells as described for other reactive lipids (32). To challenge this hypothesis in cells, we took advantage of the clickable DAC **9** (33) (**Figure 2B**). As observed for the DAC **3**, the cytotoxicity of the clickable DAC **9** was enantiospecific, biased towards (*S*)-**9**, and dependent on bioactivation by HSD17B11 (**Supplementary Figure 9A**). Cells were treated with clickable (*S*)- or (*R*)-**9** DACs, extracts prepared and click chemistry used to detect the covalent adducts of DACs onto proteins (26). Multiple modified proteins were detected in extracts from (*S*)-**9**-treated cells, while no adduct with (*R*)-**9** was detected (**Figure 3A**).

To identify the proteins lipoxidized by DACs upon bioactivation, and inspired by previous studies (34,35), we used streptavidin pull-down to isolate (*S*)-**9**-modified proteins after click chemistry-mediated ligation of a biotin handle in extracts of treated cells and identified them using bottom-up proteomics. 42 proteins were significantly enriched more than 2-fold in the (*S*)-**9** condition as compared to (*R*)-**9** (**Figure 3B**, **Supplementary File 3**), with three proteins being enriched more than 60-fold: BRAT1, PLIN3 and PSMD2. To validate the three main hits, we overexpressed BRAT1, PSMD2 and PLIN3 individually (in addition to TK1) as GFP fusions in U2OS cells (**Supplementary Figure 9B**), and used GFP pull-down to determine whether they were modified by clickable DAC **9** in cells. These proteins were found robustly modified by (*S*)-**9** but not by (*R*)-**9**, especially BRAT1 and PSMD2, while GFP alone was not modified (**Supplementary Figure 9C**).

Among the three main hits, PSMD2 drew our attention as an essential protein in HAP-1 cells (36). PSMD2, also called Rpn1, is a critical non-catalytic subunit of the 19S regulatory particle of the 26S proteasome, a large complex responsible for the ubiquitin-dependent degradation of cellular proteins. PSMD2 is essential for 19S assembly and for docking of ubiquitin, ubiquitin receptors and the deubiquitinase USP14 (37). Immunoprecipitation of endogenous PSMD2 from U2OS cells treated with clickable DAC confirmed that PSMD2 is covalently modified after treatment with the DAC (*S*)-**9** but not with (*R*)-**9** (**Figure 3C**). Moreover, the clickable DACone **10** efficiently modified

PSMD2 *in vitro* (**Supplementary Figure 9D**). Using the (*S*)-DAC-resistant HAP-1 clones A1 and A4 (expressing V16D and S172L HSD17B11 mutants, respectively), we also confirmed that the modification of cellular proteins by (*S*)-**9**, including PSMD2, was dependent on HSD17B11 (**Figure 3D** and **Supplementary Figure 9E**). Our proteomics approach also revealed that, in addition to PSMD2, a cluster of proteins involved in protein quality control (PQC) was also modified by the DAC (*S*)-**9** (**Figure 3B**), including several protein disulfide isomerases (PDIA1/P4HB, PDIA6 and TMX1), thioredoxin reductases (TXNDC5 and TXNRD1) and protein chaperones (the ER-resident HSP70, HSPA5/GRP78/BiP; and HSP90AB1), the alteration of which likely also contributes to the DAC cytotoxic effect. Altogether, these data show that (*S*)-DACs are bioactivated by HSD7B11 into highly reactive DACones that covalently lipoxidize nearby proteins, including essential proteins involved in PQC such as PSMD2, a critical subunit of the ubiquitin-proteasome system (UPS).

We then used click-based imaging to monitor the localization of DAC-modified proteins. (*S*)-**9** gave a strong nuclear and cytoplasmic staining, the latter being evocative of ER and mitochondrial membranes (**Figure 3E**). In agreement, we observed a co-occurrence of (*S*)-**9**-click staining with markers of ER (**Supplementary Figure 10A**) and mitochondria (**Supplementary Figure 10B,C**). The lack of staining in cells treated with the inactive (*R*)-**9** (**Figure 3E**) supported that the staining corresponds to DAC-modified proteins. No staining was observed with (*S*)-**3**, supporting that the -C≡CH group of the dialkynylcarbinol head is modified after bioactivation and subsequent reaction with proteins (as shown in **Figure 2I**). Since GFP-BRAT1 is the protein that was the most robustly modified by DACs in cells (**Supplementary Figure 9C**), we pre-extracted soluble proteins with mild nonionic detergent to assess GFP-BRAT1 association to subcellular compartments. Under these conditions, most GFP-BRAT1 was removed by the pre-extraction in untreated cells, as expected for a soluble protein, while it was retained to subcellular compartments evocative of ER and nucleus after treatment with (*S*)-**3** (**Figure 3F**). These data suggest that protein lipoxidation

by bioactivated DACs results, at least for some of them, into their relocalization to cellular membranes.

(*S*)-DACs trigger ER-stress, inhibition of ubiquitin-proteasome system (UPS) and apoptosis. In agreement with (*S*)-DAC impairing PQC, we observed that treatment of cells by (*S*)-**3** triggers ER swelling as shown by the appearance of a large cytoplasmic vacuole between 4 and 8 h of treatment that preceded cell death (**Figure 4A**). The use of a GFP variant targeted and retained into the ER confirmed that these vacuoles derived from this compartment (**Figure 4B**), while a mCherry protein addressed to mitochondria in the same cells showed that (*S*)-DAC treatment concomitantly triggered mitochondrial fission, a hallmark of cell stress (**Supplementary Figure 11,** see also **Supplementary movie 1**). ER swelling is a feature of ER-stress, which can result from the accumulation of unfolded proteins within the ER and can be triggered by various defects of PQC such as inhibition of the UPS, as seen with the UPS inhibitor MG132 (**Supplementary Figure 12A**). In agreement with (*S*)-**3** cytotoxicity being mediated by the accumulation of unfolded proteins, vacuolization and cell death induced by (*S*)-**3** could be blocked by inhibition of protein synthesis by cycloheximide (CHX, **Supplementary Figure 12B**). (*S*)-**3** also triggered a strong accumulation of the chaperone HSP70 and of the cell stress response protein p21, similarly to MG132 (**Figure 4C**) or PSMD2 depletion using siRNA (**Supplementary Figure 12C**). It is noteworthy that ER-stress itself can trigger UPS inhibition, likely through consuming free ubiquitin (38). In agreement with this hypothesis, we observed that (*S*)-**3** induces the accumulation of poly-ubiquitinated proteins (**Figure 4D**), a hallmark of UPS inhibition, and blocked the degradation of an artificial substrate of the UPS system in a manner similar to MG132 (**Figure 4E,F**). Similarly to MG132, (*S*)-**3** also blocked the assembly of the protein 53BP1 into foci at sites of DNA double-strand breaks (**Supplementary Figure 12D**), a process that depends on the local *de novo* DNA damage-induced ubiquitination of histones (39), thereby confirming depletion of free ubiquitin by treatment with (*S*)-**3**. It is noteworthy that (*S*)-**3** treatment itself did not induce DNA

damage nor blocked ATM activation, an important component of the DNA damage response (**Supplementary Figure 12D**). Accumulation of unfolded proteins in the ER activates the Unfolded Protein Response (UPR) which helps maintain ER protein homeostasis by reducing the influx of proteins into the ER and by increasing the activity of ER protein quality control mechanisms. The UPR is initiated by the activation of three signal transducers: IRE1α, PERK and ATF6, each controlling a specific aspect of the UPR (40). IRE1α is a ER-resident transmembrane protein, the activation of which results from its homodimerization mediated by its luminal domain, which is controlled by ER-resident chaperones including HSPA5/GRP78/BiP. IRE1α activation triggers its autophosphorylation, which is used as a marker of UPR activation. In agreement with (*S*)-**3** triggering unfolded proteins accumulation and UPR activation, we observed that treatment with (*S*)-**3** induced the rapid autophosphorylation of IRE1α, preceding the accumulation of cytoplasmic HSP70 (**Figure 4G**). Ultimately, (*S*)-**3** treatment resulted in apoptosis, as marked by PARP-1 cleavage (**Figure 4G**), in a caspase inhibitor (z-VAD-fmk)-sensitive manner (**Figure 4H**). Caspase inhibition blocked cell death but not the vacuolization process (**Supplementary Figure 12E**). Altogether, these results show that (*S*)-**3**, once bioactivated by HSD17B11, covalently modifies multiple proteins including critical components of the PQC, resulting in ER-stress, inhibition of the UPS and activation of the UPR, ultimately resulting in apoptotic cell death.

Identification of new SDR-specific prodrugs. Our discovery that an SDR, HSD17B11, bioactivates a secondary alcohol prodrug by oxidation into the corresponding ketone is particularly interesting given that the SDR superfamily is one of the largest protein superfamilies, with over 500,000 members found in most forms of life. This means that this mechanism of prodrug activation could be exploited to develop an extensive range of new drugs and compounds to kill cells or organisms expressing specific SDRs with high selectivity. SDRs use NAD(H) or NADP(H) cofactors to perform oxidoreductase, lyase or isomerase activities on a large variety of substrates including steroids, retinoic acids, lipids, polyols, sugars, nucleotides and xenobiotics (41). *In vitro*,

SDR enzymes can frequently catalyze both oxidation and reduction, depending on the supplied co-factor. In cells, however, they show directionality, which depends on their sub-cellular localization and cofactor availability. We first determined whether other SDRs with the proper *in cellulo* directional polarity could activate other secondary alkynylcarbinol-containing compounds into cytotoxic species. We found that the AAC (*S*)-**4** (with a terminal C=CH_2 group, **Figure 5A**), despite its activity being strongly reduced in DAC-resistant clone A4 (~17 fold, **Supplementary Figure 3B**), still retained some cytotoxicity (IC_{50} ~2.6 µM) on these cells, possibly through bioactivation by a second dehydrogenase. To identify such a dehydrogenase, EMS was used to mutagenize the DACR clone #A4 once again. This mutagenized population was selected with a lethal concentration of 10 µM (*S*)-**4** and over twenty resistant clones (AACR clones) were isolated. Among those, we selected seven, which all showed similar increased resistance to (*S*)-**4** (**Figure 5A**), and submitted them to RNA-seq analysis. This allowed the identification of an average of six coding mutations in each clone (**Supplementary Figure 13A**), and analysis revealed that the *RDH11* gene carried point mutations in five of these seven clones (**Supplementary Figure 13A,B**). Further analysis revealed that the clone A6 contained two alleles of *RDH11*, each with a different point mutation (**Figure 5B**), and *RDH11* expression was severely downregulated in the clone B4 (**Supplementary Figure 13C**). In conclusion, the *RDH11* gene was mutated (**Figure 5C**) or downregulated in all the AACR clones, implicating it as an SDR, with similar prodrug bioactivation capacity as HSD17B11, that mediates AAC (*S*)-**4** toxicity.

The human *RDH11* gene codes for retinol dehydrogenase 11 (also called PSDR1 or SDR7C1), a member of the SDR superfamily which also localizes to the ER (42) where it uses NADP+ to catalyze the conversion of retinol (**Figure 5D**, preferentially the 11-*cis*, all-*trans* and 9-*cis* isomers) into retinal through oxidation of the C-15 carbinol center, with a pro-*R* hydrogen specificity(43). Full-length RDH11 protein was not detectable in any of the AACR clones, suggesting that all the identified mis-sense mutations decrease RDH11 stability (**Figure 5E**). To validate the ability of

RDH11 to mediate some of the (*S*)-**4** cytotoxic effects, we compared its activity on U2OS, U2OS KO HSD17B11 and U2OS KO HSD17B11 cells in which RDH11 was inactivated using CRISPR/Cas9 (**Supplementary Figure 14A**). In this panel, we confirmed that, while HSD17B11 was responsible for the nM activity of the AAC (*S*)-**4** (48-fold IC_{50} increase as a result of HSD17B11 inactivation), the remaining toxicity of (*S*)-**4** in HSD17B11 KO cells was further decreased by inactivating RDH11 (6-fold IC_{50} increase by RDH11 inactivation, **Supplementary Figure 14B**). Comparison of the activity of (*S*)-**3** and (*S*)-**4** on U2OS KO [HSD17B11+RDH11] complemented either by HSD17B11-GFP or RDH11 (**Supplementary Figure 14C**) revealed that RDH11 bioactivates preferentially (*S*)-**4** (IC_{50}~0.28 µM, with a terminal C=CH_2 group) over (*S*)-**3** (IC_{50}~1.92 µM, with a terminal C≡CH group, **Supplementary Figure 14D**), but also established that HSD17B11 was much more efficient than RDH11 for the bioactivation of either molecule (IC_{50} < 40 nM).

As a proof-of-principle of the potential value of these discoveries for designing novel prodrugs with controlled cytotoxic activity, we attempted to design a new prodrug whose cytotoxic effects would depend more on the RDH11 SDR. We used WT U2OS or U2OS inactivated for HSD17B11, RDH11 or both (**Figure 5F**) to test several AAC analogues. Introduction of a second secondary carbinol function in the AAC structure, generating the AlkenylAlkynylDiCarbinol **12** (AADC), reduced its bioactivation by HSD17B11, while leaving intact its RDH11-dependent activation and thereby generating a new prodrug equally bioactivated by HSD17B11 and RDH11 (**Figure 5G**). As mixtures of diastereoisomers were used for this experiment, lower IC_{50} can be expected with selected AADC enantiomers, especially with the external carbinol center in the RDH11-preferred (*S*) configuration.

Another SDR, HPGD, also called 15-PGDH, PGDH1 or SDR36C1, is responsible for the inactivation of prostaglandins through oxidation of the (*S*)-C-15 carbinol center in a NAD+-dependent manner (**Figure 5H**) (44). HPGD expression is tissue-restricted (prostate and bladder)

and null in U2OS cells (*Broad Institute Cancer Cell Line Encyclopedia* RNA-seq dataset). To determine whether this SDR could also bioactivate potential prodrugs, we used U2OS inactivated for HSD17B11 and overexpressing GFP alone or HPGD-GFP (**Figure 5I**), and screened a small collection of lipidic alkynylcarbinols. We found that the AllAC (S,S_a)-**5** was selectively bioactivated by HPGD, resulting in an IC_{50} of ~147 nM in HPGD-overexpressing cells *vs* normal U2OS (**Figure 5J**). Thus, this mechanism of action is likely a general property of SDRs that could be exploited to develop a wide range of tailored prodrugs to cause selective cytotoxicity.

Discussion

Through a powerful framework (13) (see **Supplementary Note 1**), our study reveals the original mode of action of a large family of natural and synthetic cytotoxic lipids characterized by a chiral terminal functional alkynylcarbinol pharmacophore. We show that these molecules are oxidized in an enantiospecific manner by a specific SDR, HSD17B11, converting them into an alkynylketone species (ynones). Oxidation of DACs produces dialkynylketones (DACones) that proved to be highly protein-reactive electrophiles, forming *Michael* adducts with cysteines and lysines. Consequently, bioactivated DACs modify several proteins in cells, resulting in their lipoxidation by a C17 lipidic chain. Lipoxidation of a protein can modify its solubility, folding, interactions, activity and/or localization (32). In agreement, DAC treatment triggers the association of BRAT1, one of the most DAC-modified proteins, to ER and nuclear membranes (**Figure 3F**). Covalent modification of BRAT1 by the natural diterpene curcusone D was recently reported and resulted in BRAT1 degradation and reduced DNA damage response (45). Regarding (*S*)-DAC, in addition to BRAT1, multiple proteins involved in mechanisms of PQC are also lipoxidized. Considering that lipoxidation of a single protein can inhibit the UPS (46), the simultaneous modification of several critical actors of PQC is likely to result in an acute proteotoxic stress. In agreement with the general effects of protein lipoxidation, DAC treatment triggers ER-stress and inhibition of the UPS (each

one fueling the other) (38). This leads to the early activation of the UPR marked by IRE1α autophosphorylation. In addition to unfolded proteins accumulation, UPR activation could also be the result of HSPA5/GRP78/BiP lipoxidation and/or tethering of multiple proteins to ER membranes. Finally, (*S*)-DACs also quickly induce mitochondrial fission and caspase-dependent apoptosis (**Figure 6**). Of note, hundreds of known cytotoxic natural compounds have one or several alkynylcarbinol motifs. The mechanism of action identified here could thus be shared in its principles (enantiospecific bioactivation into protein-reactive lipids) by these cytotoxic molecules (see **Supplementary Note 2**).

Our work also provides a proof-of-concept that new pro-cytotoxic agents can be designed to be bioactivated through an enantiospecific oxidation catalyzed by selected SDRs. We exemplified this with three different human dehydrogenases, HSD17B11, RDH11 and HPGD (**Figure 6**). We also show here that multiple human cell lines derived from osteosarcoma, a rare pediatric cancer, were particularly sensitive to (*S*)-DACs (**Supplementary Figure 4C**), suggesting that HSD17B11- and more generally SDR-bioactivated prodrugs could find anticancer applications, especially considering that 71 different SDRs are found in humans (47). For example, HSD3B1-specific pro-drugs could prove useful to treat castration-resistant prostate cancers, since the stabilized N367T variant of this SDR, found in ~30 % of the population (rs1047303), has been associated to resistance to androgen deprivation therapies by allowing self-sufficient production of pro-proliferative androgens by prostate cancer cells (48-50).

Of note, another family of diyne molecules, the enediynes, are already used in anticancer treatments (see **Supplementary Note 3**). Beyond that, the SDR superfamily is one of the largest, with representatives in all known life forms, except viruses: 507 673 SDRs are currently identified in the Uniprot database (in 7546 species, Pfam ID: PF00106). A bioinformatic classification of SDRs has revealed that among the 314 SDR subfamilies identified (51), half are specific to bacteria. This offers the prospect of designing antibiotics with novel mechanisms of action.

Finally, our findings extend the toolbox of protein-reactive warheads with the identification of the DACone motif as a potent reactive group toward the thiol and amino groups of the side chains of cysteine and lysine, respectively. This reaction is quantitative, without co-product and operating in aqueous buffer at room temperature, making it well suited for many applications. In our study, multiple proteins could be functionalized by a terminal alkyne motif using clickable DACone **10** or **11** and the resulting linkage was found to be highly stable. The reactive species could also be readily produced *in situ* by using the appropriate SDR with its co-factor (see **Figure 2F**). Our unbiased study of the DACones reactivity using the isoDTB-ABPP approach (30) provides the first insights into the proteome-wide reactivity of these novel electrophiles. Reactive lysines have been mapped on functional domains of human proteins (52,53) and could be targeted through exploiting this new reactive entities supplied exogenously or generated *in situ*, thereby offering new avenues for protein functionalization or covalent inhibitors design.

Methods

Plasmids. Detailed information regarding the plasmids used and generated in this study are provided in the table below. Plasmids generated in this study have been produced i) by ligating annealed primers into BbsI digested plasmids (for cloning of sgRNAs) or ii) by ligating digested PCR-amplified cDNAs into dephosphorylated plasmids. Phusion DNA polymerase, FastDigest restrictions enzymes and FastAP phosphatase were used (Thermo Fisher Scientific). For all plasmids, DNA sequencing (Mix2Seq, Eurofins Genomics) was used with the specified primers, to confirm that the desired sequence was inserted. All new plasmids have been deposited on Addgene.

Plasmid name	Template for PCR-based cloning	Primers for PCR-based cloning, sequencing or oligonucleotides for annealing-based cloning	Cloned in	Cloning sites	Polymorphism	Addgene ID	Reference
ERmoxGFP						68072	(54)
Ub-G76V-YFP						11949	(38)
mCherry-Mito-7						55102	(55)
pEGFP-N1-ATG-FLAGC						60360	(56)
pEGFP-N1-HSD17B11-WT-FLAGC	RT-PCR from wild-type HAP-1	RT: HSD17B11-RNA-Rv HSD17B11-RNA-Fw Cloning: HSD17B11-F-XhoI HSD17B11-R-MluI Sequencing: SEQ-HSD17B11-F1 SEQ-HSD17B11-R1	pEGFP-N1-FLAGC, Addgene #60360 (56)	XhoI+MluI	rs6531985	161903	This work
pEGFP-N1-HSD17B11-S172L-FLAGC	RT-PCR from DACR#A4 HAP-1	HSD17B11-RNA-Rv for RT HSD17B11-F-XhoI HSD17B11-R-MluI	pEGFP-N1-FLAGC, Addgene #60360 (56)	XhoI+MluI	rs6531985	161904	This work
pICE-EGFP-FLAG-PLIN3	IMAGE clone #3833411 (Source Bioscience)	Cloning: PLIN3-F-XhoI PLIN3-R-NotI Sequencing: SEQ-GFPC-F SEQ-PLIN3-F SEQ-BGH-R	pICE-EGFP-FLAG-Ku70siR-WT; Addgene #46961 (57)	XhoI+NotI		161918	This work
pEGFP-C1-FLAG-BRAT1	IMAGE clone #3839985 (Source Bioscience)	Cloning: BRAT1-F-NotI BRAT1-R-EcoRI Sequencing: SEQ-GFPC-F SEQ-BRAT1-F1 SEQ-BRAT1-F2 SEQ-SV40PA-R	pEGFP-C1-FLAGN; Addgene #46956 (57)	NotI+EcoRI		161920	This work
pICE-EGFP-FLAG-PSMD2	IMAGE clone #2822191 (Source	Cloning: PSMD2-F-XhoI PSMD2-R-NotI Sequencing:	pICE-EGFP-FLAG-Ku70siR-WT;	XhoI+NotI		161917	This work

	Bioscience)	SEQ-GFPC-F SEQ-PSMD2-F1 SEQ-PSMD2-F3 SEQ-PSMD2-R1 SEQ-PSMD2-R2 SEQ-BGH-R	Addgene #46961 (57)				
pICE-EGFP-FLAG-TK1	IMAGE clone #2966331 (Source Bioscience)	Cloning: TK1-F-XhoI TK1-R-NotI Sequencing: SEQ-GFPC-F SEQ-BGH-R	pICE-EGFP-FLAG-Ku70siR-WT; Addgene #46961 (57)	XhoI+NotI		161919	This work
pEGFP-N1-HPGD-FLAGC	IMAGE clone #3638799 (Source Bioscience)	Cloning: HPGD-F-XhoI HPGD-R-MluI Sequencing: SEQ-CMV-F SEQ-GFPN-R	pEGFP-N1-FLAGC, Addgene #60360 (56)	XhoI+MluI		161915	This work
pE-N1-RDH11	RT PCR from wild-type HAP-1	RT: RDH11-RNA-Rv RDH11-RNA-Fw Cloning: RDH11-F-HindIII RDH11-R-NotI Sequencing: SEQ-CMV-F SEQ-SV40PA-R	pEGFP-N1-FLAGC, Addgene #60360 (56)	HindIII+NotI	rs17854678	161916	This work
pCAG-eSpCas9-2A-GFP-sgRNA-HSD17B11		Annealed primers : HSD17B11-sgRNA-S HSD17B11-sgRNA-AS Designed with Benchling Sequencing : SEQ-U6-F	pCAG-eSpCas9-2A-GFP, Addgene #79145	BbsI		161923	This work
pCAG-eSpCas9-2A-GFP-sgRNA-RDH11		Annealed primers : RDH11-sgRNA-S RDH11-sgRNA-AS Designed with Benchling Sequencing : SEQ-U6-F	pCAG-eSpCas9-2A-GFP, Addgene #79145	BbsI		161924	This work

Oligonucleotides. DNA oligonucleotides used in the study are described in the table below and were ordered from Eurofins Genomics.

ID	**Sequence 5' to 3'**	**Embedded restriction site**
Plasmid sequencing		
SEQ-CMV-F	GTAGGCGTGTACGGTGGGAGG	
SEQ-BGH-R	TAGAAGGCACAGTCGAGG	
SEQ-GFPC-F	CATGGTCCTGCTGGAGTTCGTG	
SEQ-GFPN-R	CTCCTCGCCCTTGCTCACC	
SEQ-SV40PA-R	GCAAGTAAAACCTCTACAAATGTGGTATGG	
SEQ-U6-F	TGGACTATCATATGCTTACCG	
BRAT1		
BRAT1-F-NotI	CGCGCGGCCGCATGGACCCAGAATGCGCCC	NotI
BRAT1-R-EcoRI	CGCGAATTCTCAGTAGCAGTCGGCCTCGTCC	EcoRI

SEQ-BRAT1-F1	AGAGTCCTTGTGCTCCGCGG	
SEQ-BRAT1-F2	GCCCCTGCCTCCAGTGTGG	
HPGD		
HPGD-F-XhoI	GGCCTCGAGCCACCATGCACGTGAACGGCAAAGTGG	XhoI
HPGD-R-MluI	GGCACGCGTTTGGGTTTTTGCTTGAAATGG	MluI
HSD17B11		
HSD17B11-RNA-Fw	ACACCAAACGCTCGCAGCC	
HSD17B11-RNA-Rv	CACTATTAGATGACATCAACCTAAACCTG	
SEQ-HSD17B11-F1	GAAGGTGAAGGCAGAAATTGGAG	
SEQ-HSD17B11-R1	ACATGTCCAGCTGCCGAAGC	
HSD17B11-F-XhoI	CCGCTCGAGCCACCATGAAATTTCTTCTGGACATCCTCC	XhoI
HSD17B11-R-MluI	CCGACGCGTTTGCGCTTTCATTTTATATCCAATAACTGC	MluI
HSD17B11-sgRNA-S	CACCGTGTAATCAGCACGATTTCGC	
HSD17B11-sgRNA-AS	AAACGCGAAATCGTGCTGATTACAC	
PLIN3		
PLIN3-F-XhoI	GCGCTCGAGTCTGCCGACGGGGCAGAG	XhoI
PLIN3-R-NotI	CGCGCGGCCGCCTACTTCTTCTCCTCCGGGGC	NotI
SEQ-PLIN3-F	CTGTGCAGAGCGGCGTGG	
PSDM2		
PSMD2-F-XhoI	GCGCTCGAGATGGAGGAGGGAGGCCGG	XhoI
PSMD2-R-NotI	CGCGCGGCCGCTTAGAGATCATAATTGGGGTTCTTCC	NotI
SEQ-PSMD2-F1	TGCAGAGCATGAGGCTTGCG	
SEQ-PSMD2-F3	CAGGGAGTGGCTGTTCTGGG	
SEQ-PSMD2-R1	TGTGCTCCCATGTCAGCAGG	
SEQ-PSMD2-R2	CAGCCCTCCGGAGTGTAGGC	
RDH11		
RDH11-RNA-Fw	GCTCTGGTGCCGCTGCAGCC	
RDH11-RNA-Rv	AGTCTTCTCTTGGGTCCAACTGG	
RDH11-F-HindIII	GCCAAGCTTGCCACCATGGTTGAGCTCATGTTCCCGC	HindIII
RDH11-R-NotI	CGCGCGGCCGCTTTAGTCTATTGGGAGGCCCAGCAGG	NotI
RDH11-sgRNA-S	CACCGAGTTGATGTACACACCCCAC	
RDH11-sgRNA-AS	AAACGTGGGGTGTGTACATCAACTC	
TK1		
TK1-F-XhoI	CGCCTCGAGAGCTGCATTAACCTGCCCACTGTGC	XhoI
TK1-R-NotI	CGCGCGGCCGCTCAGTTGGCAGGGCTGCATTGC	NotI

Cell lines and treatments. U2OS (ATCC), SAOS-2 (ATCC), 143B (Sigma-Aldrich), HOS (ECACC/Sigma-Aldrich), HS5 (ATCC), G292 clone 141B1 (ECACC/Sigma-Aldrich), HCT-116 (Horizon Discovery), A549 (ATCC), HT-1080 (ATCC), MDA-MB-436 (ATCC), SK-MEL-28 (ATCC), DLD-1 (ATCC), HEK293T (ATCC), MRC5-SV (ECACC/Sigma-Aldrich), HeLa (ATCC) and PC3 (ATCC) cells were grown in DMEM 10% FBS; CAPAN1 (ATCC) in IMDM 20% FBS; T47D (ATCC) and CAPAN2 (ATCC) cells in RPMI1640 10% FBS with Glutamax-I; HAP-1 (58) (Horizon Discovery) in IMDM 10% FBS and BJ-hTERT (gift from R. Weinberg, Whitehead Institute, Cambridge, USA) in DMEM 15% FBS 16% M199; human adult primary osteoblast (Cell Applications Inc., Sigma-Aldrich) in human osteoblast growth medium (Cell Applications Inc.,

Sigma-Aldrich). All cells media, except human osteoblast growth medium, contained penicillin and streptomycin (pen./strep.; Thermo Fisher Scientific) and cells were grown at 37 °C in 5% CO_2 humidified incubator. Cells were used at low passage and routinely confirmed free of Mycoplasma. Cells were treated in complete growth medium except when stated otherwise.

Plasmid transfection and stable cell generation. Cells were transfected at 90% confluency in 60 mm dishes and using 5 µg DNA and lipofectamine 2000 (Thermo Fisher Scientific) following manufacturer's instructions. The day after transfection, cells were seeded at limiting dilution in 140 mm dishes. Selection of stable transfectants was performed either with 0.4 mg/mL G418 or 0.2 µg/mL puromycin. Individual clones were isolated. Homogeneous transgene expression was confirmed by monitoring cell fluorescence (for GFP tagged constructs) or by immunofluorescence.

CRISPR/Cas9-mediated gene inactivation. Cells were transfected with pCAG-eSpCas9-2A-GFP plasmids coding for the *S. pyogenes* Cas9 K848A K1003A R1060A variant, which displays reduced off-target editing (59), and co-expressing a guide against HSD17B11 or RDH11. One week after transfection, cells could be plated at limiting dilution to perform selection of individual clones, which were analysed for proper target inactivation. Rescue experiments were performed (with HSD17B11 or RDH11) to rule out off-target-related effects.

Small-interfering RNA (siRNA)-mediated depletion. siRNA with a dTdT 3'extension were ordered from Eurofins Genomic against the following sequences: Control (Ctrl, target Firefly Luciferase) CGUACGCGGAAUACUUCGA, HSD17B11 #3 (ORF) CACAAGATCCTCAGATTGAAA, HSD17B11 #5 (3'-UTR) AACCGTTTATTTAACATATAT, PSMD2 #5 (ORF) TGGGTGTGTTCCGAAAGTTTA, PSMD2 #9 (3'-UTR) AAGGTTGTTCAATAAAGACTT. 250 000 U2OS cells were seeded in 6-well plate the day before the first transfection. The day after, cells were transfected with 50 nM of each siRNA (Control, PSMD2 or HSD17B11) for 4-5 h according to manufacturer's instruction before the medium being

479 replaced by DMEM 10% FBS without antibiotics. A second transfection was performed the day
480 after. Cells were seeded in 60 mm dishes the day before being used for experiments.

481 **Cell viability assays.** Cell viability was analyzed using SulfoRhodamine B assays (SRB). Cells
482 were seeded in 96-well plates 24 h before being treated continuously for 72 h with the indicated
483 concentration of each molecule. For the experiments described in **Figure 2C**, cells were gently
484 washed twice with PBS Ca^{2+}/Mg^{2+} just before treatment (to remove residual media), treated with
485 drugs for 1 h in PBS containing $CaCl_2$ and $MgCl_2$ (to maintain cellular adhesion), then rinsed twice
486 with complete medium (to remove residual drug), followed by a 72 h post-incubation in complete
487 culture medium. For analysis, cells were fixed for 1 h at 4 °C by addition of cold trichloroacetic
488 acid at a 3.33% final concentration. After being washed four times with water and dried, cells were
489 stained by a 30 min incubation in a solution of 0.057% (wt:vol) SRB in 1% acetic acid. The wells
490 were washed four times with 1% acetic acid, dried and the dye was resuspended by a 2 h
491 incubation in a 10 mM Tris-Base solution. Absorbance at 490 nm of each well was measured
492 (μQuant plate reader, Bio-tek) and used as a readout of cell number. For calculation, background
493 absorbance was subtracted to each value and the data were normalized to the value measured
494 in untreated wells. Each point was measured in duplicate and the graphs correspond to at least
495 three independent experiments. IC_{50} were computed with the GraphPad Prism software using a
496 non-linear regression to a four-parameter logistic curve (log[inhibitor] *vs* response; variable slope).

497 **Analysis of RNA expression levels in published dataset.** The data visualization tool Ordino
498 (60) was used to compare the RNA expression levels of selected genes in The Cancer Cell Line
499 Encyclopedia RNA-seq dataset (http://www.broadinstitute.org/ccle(22)).

500 **Mutagenesis and selection with (*S*)-3 and (*S*)-4.** 100.10^6 haploid HAP1 cells at 60 % confluency
501 were treated for 72 h with 0.3 mg/mL ethyl methanesulfonate (EMS, Sigma-Aldrich) directly added

to the cell medium. After recovery, two 140 mm dishes at 10^6 cells/dish were seeded from this mutagenized population and selected by treatment with 0.25 µM DAC (*S*)-**3** for 72 h. After treatment, the medium was refreshed and, after 2-3 weeks, individual clones were isolated (DACR clones). To isolate AACR clones, the DACR clone #A4 at early passage was mutagenized again (0.3 mg/ml EMS for 72 h). After recovery, the mutagenized DACR population was seeded into 140 mm dishes (10^6 cells/dish) and selected by treatment with 10 µM (*S*)-**4** for 72 h. After treatment, the medium was refreshed and, after 2-3 weeks, individual clones were isolated (AACR clones).

RNA-seq. RNA-seq was performed at the GeT-PlaGe core facility, INRA Toulouse, from total RNA prepared with the RNeasy Plus Mini Kit (Qiagen) according to the manufacturer's instructions. RNA-seq libraries were prepared according to Illumina's protocols using the Illumina TruSeq Stranded mRNA sample prep kit. Briefly, mRNAs were selected using poly-dT beads. Then, RNAs were fragmented and adaptors ligated. Eleven cycles of PCR were applied for library amplification. Library quality was assessed using a Fragment Analyzer System (Agilent) and libraries were quantified by Q-PCR using the Kapa Library Quantification Kit (Roche). RNA-seq experiments were performed on an Illumina HiSeq3000 using a paired-end read length of 2x150 pb. RNA-seq data have been deposited on SRA (Bioproject IDs PRJNA668246 & PRJNA668322).

RNA-Seq alignment and SNP prediction and filtering. Read quality was confirmed within the ng6 environment(61) using fastQC (http://www.bioinformatics.babraham.ac.uk/projects/fastqc/) and Burrows-Wheeler Aligner BWA (62) to search for contamination. The reads were cleaned with cutadapt v1.8.3 and aligned against hg38 reference human genome with STAR v2.5.2b (63). Expression levels were computed with featureCounts (64) using Ensembl annotation. Alignments were deduplicated with samtools rmdup and reads not uniquely mapped removed. Then GATK v3.5 base quality score recalibration was applied (65). Indel realignment, SNP and INDEL discovery were performed with HaplotypeCaller using standard hard filtering parameters

526 according to GATK best practices recommendations for RNAseq. Finally variants were annotated
527 using snpEff v4.3t (66). A python script was used to select protein coding variants specific to
528 resistant clones as compared to the parental HAP-1 (wild-type for DACR clones, and DACR#A4
529 for AACR clones) with a minimal allele frequency of 0.9 and a depth greater than 10 reads. Among
530 these variants, were selected the ones that resulted in frameshifts, mis- and non-sense mutations
531 as compared to the reference human genome hg38. Cytoscape v3.2.0 (67) was used to identify
532 genes found mutated in several clones and to generate a graphical overview.

533 **Targeted sequencing of HSD17B11 cDNA from HAP-1 clones.** Total RNAs were extracted
534 from wild-type or DACR HAP-1 with the RNeasy Plus Mini Kit (Qiagen) according to the
535 manufacturer's instructions. HSD17B11 cDNA was produced from these RNAs with the
536 Superscript III First-Strand kit (Thermo Fisher Scientific) according to the manufacturer's
537 instructions and using the HSD17B11-RNA-Rv primer. The resulting HSD17B11 cDNAs was
538 amplified using the primer pair HSD17B11-RNA-Fw – HSD17B11-RNA-Rv and sequenced using
539 the primers HSD17B11-SEQ-F and HSD17B11-SEQ-Rv (Eurofins Genomics).

540 **Antibodies.** For immunoblotting, horse-radish peroxidase-conjugated goat anti-mouse or anti-
541 rabbit secondary antibodies (Jackson Immunoresearch Laboratories), or IRDye800CW-
542 conjugated donkey anti-mouse or anti-rabbit secondary antibodies (LI-COR Biosciences) were
543 used, diluted at 1/10000 in PBS 0.1% Tween-20. For immunofluorescence, AlexaFluor488- or
544 AlexaFluor594-conjugated goat anti-mouse or anti-rabbit antibodies (Thermo Fisher Scientific)
545 were used diluted at 1/1000 in blocking buffer. A list of primary antibodies used in this study,
546 together with related information is provided in the table below (I.B., Immunoblotting; I.F.,
547 Immunofluorescence; * RDH11 antibody was used in immunofluorescence to check
548 homogeneous RDH11 expression in complemented cells).

549

Target	Type	Clone/Ref.	Raised in	Source	Dilution for I.B.	Dilution for I.F.
53BP1	Polyclonal	NB100-304	Rabbit	Novus Biologicals		1/800
β-Actin	Monoclonal	MAB1501	Mouse	Chemicon	1/20000	
BRAT1	Polyclonal	A300-728A	Rabbit	Bethyl laboratories	1/700	
COXIV	Monoclonal (AlexaFluor594 conjugate)	3E11	Rabbit	Cell signaling		1/50
GFP	Monoclonal	7.1 + 13.1	Mouse	Roche	1/2000	
H2AX	Polyclonal	ab11175	Rabbit	Abcam	1/4000	
gH2AX	Monoclonal	JBW301	Mouse	Millipore		1/1000
HPGD	Polyclonal	HPA005679	Rabbit	Sigma-Aldrich	1/100	
HSD17B11	Polyclonal	16303-1-AP	Rabbit	Proteintech	1/250	
HSP70	Polyclonal	10995-1-AP	Rabbit	Proteintech	1/3000	
IRE1α-Ph S724	Polyclonal	NB100-2323SS	Rabbit	Novus Biologicals	1/1000	
Ku80	Monoclonal	Clone 111	Mouse	Thermo	1/200	
p21 WAF1/CIP1	Polyclonal	sc-397-G / C-19	Goat	Santa Cruz	1/100	
PARP-1	Polyclonal	#9542	Rabbit	Cell Signaling Tech.	1/1000	
PSMD2	Polyclonal	A303-854A-T	Rabbit	Bethyl laboratories	1/700	
RDH11	Monoclonal	Clone 1B4 / GTX83716	Mouse	GeneTex	1/1000	1/200*
SAFA	Monoclonal	3G6	Mouse	Santa Cruz	1/100	
Ubiquitin	Monoclonal	Clone VU-1	Mouse	LifeSensors	1/1000	

Live imaging. Pictures of living cells were acquired using an Olympus IX73 fluorescence microscope fitted with a 40X objective (0.75NA UPlanFLN, Olympus) or a 20X 0.40 NA objective (LCAChN 0.4NA, Olympus), a X-Cite Series 120Q lamp (Lumen dynamics), a DP26 camera (Olympus) and using the adequate filters set. For time series, cells were seeded in glass-bottom dishes (from MatTek or ibidi µSlide) in phenol red-free Leibovitz's L-15 medium containing 10% FBS and pen./strep. For each time point, z-stacks were acquired using a Andor/Olympus Yokogawa CSU-X1 confocal spinning disk fitted with 60X (UPLSAPO NA 1.35, Olympus) or 100X (UPLSAPO NA 1.4, Olympus) objectives, a Andor iXon Life 888 EM-CCD camera and with temperature and humidity control. The white scale bars on representative pictures represent 10 µm.

Immunofluorescence. Cells were seeded on glass coverslips (#1.5 thickness; ~170 µm, VWR). At the end of the treatment, the cells were washed twice with PBS, fixed by a 15 min incubation with 2% paraformaldehyde (PFA) in PBS and washed three times. The cells were then

permeabilized 5 min with 0.2% Triton X-100 in PBS and washed three times with PBS. The coverslips were incubated 10 min in blocking buffer consisting in PBS 0.1% Tween-20 (PBS-T) containing 5% bovine serum albumin (BSA). The coverslips were incubated for 75 min with the primary antibodies diluted in blocking buffer (mouse anti-γH2AX antibody at 1/1000 and rabbit anti-53BP1 at 1/800), washed four times in PBS-T and then incubated 45 min with the secondary antibodies diluted in blocking buffer, washed four times in PBS-T and twice in PBS, incubated 15 min with 2 µg/mL DAPI (4′,6-diamidino-2-phenylindole) in PBS, washed twice with PBS, dipped in double-distilled water and mounted in VectaShield on a glass slide. Pictures were acquired using an Olympus IX73 microscope fitted with a 40x UPlanFLN objective (Olympus), a X-Cite Series 120Q lamp (Lumen dynamics), a DP26 camera (Olympus) and using the adequate filters set. The white scale bars on each picture represent 10 µm.

Immunoblotting. For whole-cell extracts (WCE), cells were washed with cold PBS and scrapped in 75 µL SDS-lysis buffer (120 mM Tris-HCl pH 6.8, 20% glycerol, 4% SDS), incubated 5 min at 95 °C and passed 10 times through a 25G needle. Measuring the absorbance at 280 nm with a Nanododrop spectrometer (Thermo Fisher Scientific) was used to evaluate protein concentration and, after adjustment with SDS-Lysis buffer, extracts were diluted by addition of equal volume of SDS-Loading Buffer (5 mM Tris pH 6.8, 0.01% bromophenol blue, 0.2 M dithiothreitol). Immunoblotting was performed with 25-50 µg of WCE. Proteins were separated on gradient gels (BioRad 4-12% TGX pre-cast gels) and transferred onto Protran 0.45 µm nitrocellulose membranes (GE Healthcare). After transfer, membranes could be scanned with an infrared imager (Odyssey, LI-Cor Biosciences) to acquire the signal from AlexaFluor647 modified proteins. Homogeneous loading and transfer were checked by Ponceau S staining. When necessary, membranes were cut into horizontal strips to simultaneously probe for multiple proteins. For immunoblotting, membranes were blocked with PBS containing 5% non-fat dry cow milk, washed and incubated for 1-2 h at room temperature or 16 h at 4 °C with primary antibodies diluted in

PBS-T containing 1% bovine serum albumin (immunoglobulin- and lipid-free fraction V BSA, Sigma-Aldrich). After extensive washes, membranes were probed 1 h at room temperature with adequate secondary antibodies coupled with horse-radish peroxidase (HRP) or with IRDye800CW. For HRP-conjugated secondary antibodies, signal acquisition was performed with a CCD camera (Chemidoc, BioRad) or using autoradiographic films (Blue Devil, Genesee Scientific) after incubation with peroxidase chemiluminescent substrates (BioRad Clarity ECL for CCD acquisition; Advansta WesternBright ECL for autoradiographic film exposure). For IRDye800CW-coupled secondary antibodies, membranes were scanned using an infrared imager (Odyssey, LI-Cor Biosciences).

Analysis by SDS-PAGE of proteins modified by DACs in cells. Sub-confluent 140 mm dishes, seeded two days before with U2OS or HAP-1 cells, were treated for 2 h with 2 µM of DAC. At the end of treatment, cells were collected by trypsination and centrifugation (900 RPM, 4 °C, 5 min). The cell pellet was washed with cold PBS before being lysed by sonication on ice (Vibracell, Bioblock Scientific, ten 2s-pulses, of amplitude 30) in 400 µL of IPL buffer (20 mM Tris-HCl pH 7.8, 1 mM EDTA, 150 mM NaCl, 0.5% IGEPAL CA-630, HALT proteases and phosphatases inhibitor cocktail (Thermo Fisher Scientific)). A centrifugation (15000 RPM, 4 °C, 4 min) was used to remove insoluble material and the supernatant was used for click reactions. The click reaction was performed by incubation at 20 °C for 30 h of a mix containing 240 µg of proteins (diluted in 10 µL IPL buffer), 4 mM $CuSO_4$, 5 µM azido-AlexaFluor647 and 10 mM sodium ascorbate in IPD buffer (20 mM Tris-HCl pH 7.8, 1 mM EDTA, 150 mM NaCl, 0.05% IGEPAL CA-630, HALT inhibitors cocktail) to reach 80 µL. 20 µL of 5XLoading Buffer (300 mM Tris-HCl pH 6.8, 5% SDS, 0.025% bromophenol blue, 15% glycerol, 250 mM dithiothreitol) was added at the end of the reaction, followed by incubation at 95 °C for 5 min. 24 µg of proteins were separated on SDS-PAGE gels (BioRad 4-15% TGX pre-cast gels), followed by transfer onto Protran 0.45 µm

nitrocellulose membranes (GE Healthcare) which were scanned on an infrared imager (Odyssey, LI-COR Biosciences). A ponceau S staining was used to control for homogeneous loading.

Immunoprecipitation (IP). For IP, U2OS and HAP-1 parental or overexpressing GFP-tagged protein cell lines were seeded in 140 mm dishes two days before treatment. Sub-confluent cells were treated (or not) with the indicated molecules for 2 h. At the end of treatment, cells were collected by trypsination and centrifugation (900 RPM, 5 min, 4 °C). The cell pellet was washed with cold PBS before being lysed by sonication on ice (Vibracell, Bioblock Scientific, ten 2s-pulses, of amplitude 30) in 400 µL of IPL buffer (20 mM Tris-HCl pH 7.8, 1 mM EDTA, 150 mM NaCl, 0.5% IGEPAL CA-630, HALT proteases and phosphatases inhibitor cocktail (Thermo Fisher Scientific)). A centrifugation (15000 RPM, 4 °C, 4 min) was used to remove insoluble material and the supernatant was used for IP. IP were performed by incubation of lysates 4 h at 4 °C on a rotating wheel with either 50 µL of DynaBeads M-280 protein A magnetic beads (Thermo Fisher Scientific), pre-loaded with 8 µg of rabbit control (Dako) or anti-PSMD2 (Bethyl Laboratories) antibodies, or with 50 µL of anti-GFP magnetic beads (GFP-Trap, Chromotek). Each IP was done on 240 µg of proteins diluted in 220 µL of IPL buffer to which 480 µL of IPD buffer was added (to dilute IGEPAL CA-630 to ~0.15%). On-bead protein modification by DACones could be performed at that stage (see below). Then the beads were washed 3 times with high-salt IPW buffer (20 mM Tris-HCl pH 7.8, 1 mM EDTA, 500 mM NaCl, 0.05% IGEPAL CA-630, HALT inhibitors cocktail) and once with IPD buffer (with 500 µL for each wash).

On-bead protein modification by DACones. After IP, beads were washed twice in MoD buffer (10 mM phosphate pH 7.4, 2.7 mM KCl, 137 mM NaCl, 0.05% IGEPAL CA-630, HALT proteases and phosphatases inhibitor cocktail). Reactions with DACones were performed by incubating the beads 30 min at 30 °C with vigorous intermittent shaking in 400 µL of MoD buffer containing 1 µM DAC (*S*)-**9** or DACone **10**. Beads were then washed with IPW buffer as described above and clicked as described below.

On-bead click with azido-AlexaFluor647. Immunopurified proteins were clicked on beads by a 30 min-incubation at 20 °C with vigorous intermittent shaking in 200 µL of IPD buffer containing 4 mM $CuSO_4$, 5 µM azido-AlexaFluor647 and 10 mM sodium ascorbate. The beads were washed with IPD buffer and resuspended in 20 µL SDS-Lysis Buffer to which 20 µL of SDS Loading buffer was added. Beads were incubated 5 min at 95 °C in this solution and 20 µL of supernatant was analyzed on gradient gels (BioRad 4-12% TGX pre-cast gels). The modified proteins were detected with an infrared imager (Odyssey, LI-COR Bioscience) after transfer onto a nitrocellulose membrane (Protran, 45 µm pores, GE Healthcare) and total proteins on the membrane were stained with Ponceau S.

***In vitro* protein modification by DACones for analysis by SDS-PAGE.** FBS (Euromedex), bovine serum albumin (BSA, A-7030, Sigma-Aldrich), bovine carbonic anhydrase (CANH, C-3934, Sigma-Aldrich), Jack bean concanavalin A (ConcA, C-2010, Sigma-Aldrich), bovine beta-lactoglobulin (BLG, L-3908, Sigma-Aldrich) were resuspended at 2 mg/mL in MoD buffer. Reactions were performed for 40 min at 30 °C in 50 µL of MoD buffer containing 20 µg of protein and 2 µM of DAC or DACone. The reactions were then diluted to 75 µL by sequential addition of IPD buffer, $CuSO_4$, azido-AlexaFluor647 and sodium ascorbate to a final concentration of 4 mM, 4 µM and 10 mM, respectively and incubated 30 min at 20 °C with vigorous intermittent shaking. At that stage, unclicked azido-AlexaFluor647 could be removed using BioRad MicroBioSpin P-6 columns equilibrated with SDS-Lysis buffer and following manufacturer's instructions. Then, 8 µL of the click reaction medium were supplemented with 12 µL of SDS-Lysis buffer and 20 µL of SDS Loading buffer, incubated 5 min at 95 °C and separated on gradient gels (BioRad 4-12% TGX pre-cast gels). The modified proteins could be detected with an infrared imager (Odyssey, LI-COR Biosciences) directly in the gel or after transfer onto a nitrocellulose membrane. Total proteins in the gel or on the membrane were visualized using Coomassie (Instant*Blue*, Sigma-Aldrich, scanned with the Odyssey or BioRad Chemidoc imagers) or Ponceau S staining, respectively.

***In vitro* DAC bioactivation assays.** HSD17B11 was immunopurified from UO2S KO HSD17B11 complemented either with HSD17B11-GFP wild-type or the S172L mutant. After extensive washes with a buffer containing 500 mM NaCl, the magnetic beads were used as a source of HSD17B11 enzyme. HSD17B11 is a membrane-anchored protein (17) and its activity required maintaining a minimal 0.2% IGEPAL CA-630 concentration in all the buffers. In details, after IP, 30 µL of beads were washed twice with MoD buffer and incubated 30 min at 30 °C with vigorous intermittent shaking in 50 µL of MoD buffer containing 0.2% IGEPAL CA-630, 1 mM β-NAD+, 2 µM (*S*)- or (*R*)-**9** and 40 µg of beta-lactoglobulin (BLG, L-3908, Sigma-Aldrich). The reactions were then diluted to 75 µL by sequential addition of MoD buffer, $CuSO_4$, azido-AlexaFluor647 and sodium ascorbate to final concentrations of 4 mM, 3 µM and 10 mM, respectively. The click reaction was performed by incubation 30 min at 20 °C with vigorous intermittent shaking. 8 µL of supernatant, containing the BLG, was supplemented with 12 µL of SDS-Lysis and 20 µL SDS Loading buffer, incubated 5 min at 95 °C before analysis by SDS-PAGE and transfer onto a nitrocellulose membrane (Protran, 45 µm pores, GE Healthcare). DACone adducts onto BLG were visualized by scanning the membrane with an infrared imager (Odyssey, LI-COR Biosciences) and total protein stained with Ponceau S.

MS analysis of entire β-lactoglobulin modified by DACone. Commercially available purified BLG (mixture of isoforms A and B) was incubated for 40 min at 30 °C in 40 µL of MoD buffer containing 30 µM BLG and 100 µM DACone **10** (or the same volume of acetonitrile as control, 10% final concentration). Prior to MS analysis, unmodified and modified BLG samples were desalted in 200 mM ammonium acetate, pH 7 using BioRad Micro Bio-Spin 6 devices and diluted to ~4 µM in 50% acetonitrile plus 0.2% formic acid final. Samples were analyzed on a SYNAPT G2-Si mass spectrometer (Waters, Manchester, UK) running in positive ion mode and coupled to an automated chip-based nano-electrospray source (Triversa Nanomate, Advion Biosciences, Ithaca, NY, USA). The voltage applied to the chip and the cone voltage were set to 1.6 kV and

150 V, respectively. The instrument was calibrated with a 2 mg/mL cesium iodide solution in 50% isopropanol. Raw data were acquired with MassLynx 4.1 (Waters, Manchester, UK) and deconvoluted with UniDec using the following parameters: m/z range: 1,300-2,800 Th; subtract curved: 1; Gaussian smoothing: 10; bin every 1 Th; charge range: 5-15; mass range: 18,000-19,000 Da; sample mass: every 1 Da; peak FWHM: 1 Th; peak detection range: 50 Da, and peak detection threshold: 0.1. The mass spectrometry proteomics data have been deposited to the ProteomeXchange Consortium via the PRIDE (68) partner repository with the data set identifier PXD021955.

isoDTB-ABBP-based framework for assessing the proteome-wide selectivity of DACones. Total cell extracts from U2OS cells were prepared by sonicating in 5 mL of PBS 0.1% IGEPAL CA-630 containing protease and phosphatase inhibitors (HALT cocktail, Pierce) a pellet of 1.5 mL of U2OS cells, collected by scrapping in cold PBS, followed by centrifugation 30 min at 15000 RPM at 4°C. Protein concentration in the supernatant was evaluated using a Nanodrop device (Thermo Fisher Scientific) and the extracts diluted at 1 mg/mL with PBS containing protease and phosphatase inhibitors. 1 mL of extracts was incubated for 40 min at 30°C with 100 µM of DACone **10** or **11** or acetonitrile (1% final, solvent control). Proteins were then precipitated overnight at -20°C by addition of 4 volumes of cold acetone followed by centrifugation at 16000 g for 15 min at 4°C. The precipitates were resuspended in 1 mL cold MeOH by sonification and centrifuged (10 min, 21100 ×g, 4 °C). The supernatant was removed and the washing step with MeOH was repeated once. The pellets were dissolved in 1 mL 0.8% SDS in PBS by sonification. Duplicates were performed for each condition, one being clicked with the heavy isoDTB tag, the other one with the light tag. The click reaction, all subsequent experimental and analytical steps were performed as described (30). The data presented correspond to two independent experiments (Exp.1 and 2 in **Supplementary Files 1 and 2**). PSSM sequence logos were generated by analyzing the 10 amino acids surrounding the modified site using Seq2Logo (69). The mass

spectrometry proteomics data have been deposited to the ProteomeXchange Consortium via the PRIDE (68) partner repository with the data set identifier PXD021955.

Reaction of DACone with purified proteins for analysis of the absorbance spectrum. Reactions were performed by incubation at 30 °C for 40 min in 30 µL of MoD buffer containing 115 µg of protein (equivalent to 0.1 mM BLG and 0.035 mM BSA) and 0.3 mM of DAC or DACone. 2 µL of each reaction were used to acquire a UV-visible (190-840 nm) absorbance spectrum on a Nanodrop device (Thermo Fisher Scientific).

Reaction of DACones with NAG, NAC and NAK for analysis of the absorbance spectrum. Reactions were performed by incubation at 30 °C for 40 min in 40 µL of a mixture containing 1 mM NAG, NAC or NAK and 1 mM DACone **8** in 20 mM phosphate buffer (pH 7.4) or 10 mM KOH (pH 10). A UV-visible (190-840 nm) absorbance spectrum for each reaction was acquired using a Nanodrop spectrometer (Thermo Fisher Scientific).

NMR characterization of DACone reaction products with N_α-Acetyl Lysine and *N*-Acetyl Cysteine. Reactions were performed by incubating at 30 °C for 40 min a 300 µL mixture containing 20 mM DACone **8**, 20 mM NAC or 20 mM NAK and 10 mM KOH (pH 10) or 20 mM phosphate buffer (pH 7.2). Each reaction was characterized by high-resolution mass spectrometry. After lyophilization, the samples were dissolved at a concentration of 10 mM in PBS buffer pH 7.4 with 10% D_2O containing DSS at 1 µM. All compounds were fully characterized by ^{1}H and ^{13}C NMR spectroscopy. NMR spectra were recorded at 298 K on Avance III HD 700 spectrometer (^{1}H: 700.13 MHz, ^{13}C: 176.04 MHz). ^{1}H NMR spectra were recorded with water suppression. The correlation ^{1}H spectroscopy was acquired with the Bruker pulse sequence dipsiesgp using an excitation sculpting sequence for water suppression. The recycle delay was set to 1.5 s. ^{1}H-^{13}C HSQC experiment (Bruker pulse sequence hsqcphpr) was recorded with carrier frequencies set to 4.7 ppm (^{1}H) and 85 ppm (^{13}C) and the spectral widths were set to 12 ppm (^{1}H) and 180 ppm

(^{13}C). For this experiment, the recycle delay was set to 1 s. Spectral data are provided in **Supplementary Figure 8** and **Supplementary Note 5**.

Identification of proteins modified by DAC (*S*)-9 in cells. Two 140 mm dishes, seeded with $2.5x10^6$ U2OS cells two days before, were treated for 2 h with 2 µM of DAC (*S*)-**9** or (*R*)-**9**. At the end of treatment, cells were collected by trypsination and centrifugation (900 RPM, 4 °C, 5 min). The cell pellet was washed with cold PBS before being lysed by sonication on ice (Vibracell, Bioblock Scientific, ten 2s-pulses, of amplitude 30) in 240 µL of IPL buffer (20 mM Tris-HCl pH 7.8, 1 mM EDTA, 150 mM NaCl, 0.5% IGEPAL CA-630, HALT proteases and phosphatases inhibitor cocktail (Thermo Fisher Scientific)). A centrifugation (15000 RPM, 4 °C, 4 min) was used to remove insoluble material and the supernatant was used for click pull-down. A volume of lysate corresponding to 300 µg of proteins was diluted to 500 µL with IPD buffer (20 mM Tris-HCl pH 7.8, 1 mM EDTA, 150 mM NaCl, 0.05% IGEPAL CA-630, HALT inhibitors cocktail) bringing IGEPAL CA-630 concentration to 0.2-0.25%. The lysate was pre-cleared by incubation with 60 µL streptavidin-coupled magnetic beads (Dynabeads M-280, Thermo Fisher Scientific) 1 h at 4 °C on a rotating wheel. Then $CuSO_4$, biotin-azido and sodium ascorbate were added to the pre-cleared lysate at 4 mM, 5 µM and 10 mM final concentration, respectively. The click-reaction was performed by incubation for 30 min at 20 °C in the dark with vigorous intermittent shaking and the free biotin was removed from the clicked extracts using PD MiniTrap G-25 column (GE Healthcare) equilibrated with IPD buffer. The extracts were then complemented to 600 µL with IPD buffer and incubated for 2 h at 4 °C on a rotating wheel with 60 µL of streptavidin-coupled magnetic beads (Dynabeads M-280, Thermo Fisher Scientific). The beads, corresponding to the proteins associated to (*S*)- or (*R*)-**9**, were then washed extensively with high-salt IPW buffer (20 mM Tris-HCl pH 7.8, 1 mM EDTA, 500 mM NaCl, 0.05% IGEPAL CA-630, HALT inhibitors cocktail), then with IPD buffer. For on-bead trypsic digestion, beads were washed twice with 50 mM ammonium bicarbonate buffer, and then suspended in 7 M urea and 25 mM DTT (Sigma-Aldrich). After 60

762 min under agitation (850 rpm) at room temperature, the samples were alkylated by incubation in
763 90 mM iodoacetamide (Sigma-Aldrich) during 30 min in the dark. Samples were then washed
764 twice as described above and submitted to overnight proteolysis in ammonium bicarbonate buffer
765 containing 1 µg of trypsin (Promega) per sample at 37 °C. The supernatants were collected, dried
766 in speed-vac and resuspended with 2% acetonitrile and 0.05% trifluoroacetic acid (Sigma-Aldrich),
767 for mass spectrometry analysis. The resulting peptides were analyzed with a NanoLC (Ultimate
768 3000 RSLCnano system Thermo Scientific) coupled to a LTQ Orbitrap Velos mass spectrometer
769 (Thermo Fisher Scientific, Bremen, Germany). Raw MS files were processed with MaxQuant
770 v1.5.2.8 software for database search with the Andromeda search engine and quantitative
771 analysis. Data were searched against human entries in the Swissprot protein database. To
772 perform relative quantification between proteins identified, we used the LFQ from the MaxQuant
773 "protein group.txt" output. The experiment was repeated three times (exp. #1, #2 and #3 in
774 **Supplementary File 3**). The mass spectrometry proteomics data have been deposited to the
775 ProteomeXchange Consortium via the PRIDE (68) partner repository with the data set identifier
776 PXD021955. For each protein identified, the ratio (*S*)-**9** vs (*R*)-**9** conditions was computed (fold
777 change, FC) and a t-test was used to select proteins reproductively enriched (FC > 2 and $p < 0.05$)
778 in the (*S*)-**9** vs (*R*)-**9** condition. Cytoscape(67) was used to generate **Figure 3B** visual
779 representation, in which the FC is color-coded, while the -log(p) was used to define protein box
780 size (*id* large box means highly significant enrichment).

781 **Click-based imaging, GFP fluorescence and immunofluorescence imaging, pre-extraction.**
782 Cells were seeded on #1.5 glass coverslips (VWR) the day before the experiment. For labelling
783 mitochondria with MitoTracker, MitoTracker Red CMXRos (Thermo Fisher Scientific) was added
784 at 0.2 µM in complete medium 30 min before the end of the treatments. To monitor the association
785 of GFP-BRAT1 to insoluble compartments, cells were pre-extracted at the end of the treatment by
786 a 2 min incubation on ice in cold PBS 0.1% Triton X-100 containing HALT proteases/phosphatase

inhibitors cocktail. At the end of treatments or after pre-extraction, cells were washed twice with PBS, fixed 15 min with 2% PFA in PBS and washed three times with PBS. Cells were permeabilized by incubation 8 min in PBS 0.2% Triton X-100 before being washed three times with PBS. When co-staining with antibody was performed, cells were incubated 10 min in IF blocking buffer (PBS-T 5% BSA), before being incubated 75 min with AlexaFluor594-coupled anti-COXIV antibody diluted at 1:50 in IF blocking buffer. For co-staining of ER membranes with concanavalin A, fixed cells were incubated 30 min AlexaFluor488-coupled concanavalin A diluted at 100 µg/mL in blocking buffer. At the end of antibody/concanavalin staining, cells were washed four times, fixed for 15 min, washed three times with PBS and incubated in blocking buffer. Click with AlexaFluor488-azido or AlexaFluor594-azido was performed as described (70). At the end of the procedure, cells were washed four times with PBS-T, twice with PBS and incubated 15 min in PBS containing 2 µg/mL DAPI (Sigma-Aldrich). The coverslips were washed twice with PBS and mounted with VectaShield (Vector laboratories) on glass slides. Images were acquired on a Deltavision PersonalDV microscope (Applied Precision, 1024x1024 CoolSNAP HQ, z-stack of 0.2 µm interval) equipped with a 100x UPlanSApo/1.40 oil objective (Olympus) or with a Zeiss Elyra 7 3D Lattice SIM super-resolution microscope fitted with a 63X objective (PLANAPO NA 1.4, Zeiss) and dual sCMOS cameras (pco.edge). Deconvolutions were then performed with SoftWoRx (Applied Precision) in conservative mode while 3D-SIM reconstruction were performed with Zen Black (Zeiss). The white scale bars on representative pictures represent 10 µm.

Flow cytometry. U2OS stably expressing the UPS fluorescent reporter Ub-G76V-YFP (38) were treated for 4 h with 20 µM MG132 or 1 µM (*S*)-**3**. At the end of the treatment, cells were collected by trypsination, washed in PBS 1% BSA and fixed by incubation at room temperature in 500 µL of 2% PFA in PBS. Cells were washed with PBS 1% BSA and stored in the same buffer. A minimum of 30 000 cells were analyzed on BD LSR II flow cytometer (Becton Dickinson). Data

were analyzed and formatted using FlowJo v8.8.7. Untreated cells were used to define a gate to identify the YFP positive cells in the treated conditions.

Synthesis. Synthesis and characterization of (*S*)-**1***(8),* (*R*)-**1***(8)*, (*R*)-**2**(8), (*S*)-**3**(8), (*R*)-**3**(8), (*S*)-**4***(8)*,(*R,Sa*)-**5***(19)*, (*S, Sa*)-**5***(19)*, (*S*)-**6***(20)*, (*S*)-**9**(33), (*R*)-**9**(33) have been described previously. Enantiomeric (ee) and diasteromeric (de) excesses of aforementioned compounds are the following: (*S*)-**1** (90% ee), (*R*)-**1** (80% ee), (*R*)-**2** (80% ee), (*S*)-**3** (91% ee), (*R*)-**3** (93% ee), (*S*)-**4** (91% ee), (*R,Sa*)-**5** (98% ee, 91% de), (*S,Sa*)-**5** (89% ee, 74% de), (*S*)-**6** (89% ee), (*S*)-**9** (97% ee), (*R*)-**9** (73% ee). Synthesis and characterization of new compounds is described in **Supplementary Note 4** and NMR spectra of all new compounds are provided in **Supplementary Note 6**.

Data availability. RNA-seq data, proteomics data and plasmids have been deposited on SRA, PRIDE and Addgene, respectively. All other data are available upon request.

Acknowledgements

We are grateful to the Genotoul bioinformatics platform Toulouse Occitanie and TRI-IPBS Imaging Core Facility, member of TRI-Genotoul, for providing help, computing and storage resources. The NMR spectra were recorded on spectrometers of the Integrated Screening Platform of Toulouse (PICT, IBISA). We thank Laurence Nieto (team C. Muller, IPBS, Toulouse, France), Raphaël Rodriguez (Institut Curie, Paris, France), Frédérique Fallone (Team C. Muller, IPBS, Toulouse, France), Frédéric Deschaseaux (STROMALab, Toulouse, France), Pierre Cordelier (CRCT, Toulouse, France), Robert A. Weinberg (Whitehead Institute, Boston, USA), Erik Snapp (HHMI's Janelia Research Campus, Ashburn, USA), Nico Dantuma (Karolinska Institutet, Stockholm, Sweden) for the generous gift of reagents; Antonio Peixoto & Emmanuelle Näser (IPBS, Toulouse, France) for technical assistance; Andreas Merdes (CBI, Toulouse) for providing access to his microscope. We gratefully acknowledge Stephan A. Sieber and his group for their generous support. This study was funded by the grants IDEX Transversalité "Fishing Sponge" (2015 program) from Université Paul Sabatier; N°PJA 20171206477 from "Fondation ARC", ANR-17-CE18-0002-01 from "Agence Nationale de la Recherche" and CAPES-COFECUB Ph-C n° 883/17. The GeT and proteomics facilities received funding from "Investissements d'avenir" program as part of the "Genomic French Infrastructure" (grant ANR-10-INBS-09) and the "Proteomics French Infrastructure" (grant ANR-10-INBS-08 to O.B.-S.), respectively. The Proteomics facility received financial support from the "Fonds Européens de Développement Régional Toulouse Métropole and the Région Midi-Pyrénées" (to O.B.-S.). S.M.H. and P.R.A.Z. acknowledge funding by the Fonds der Chemischen Industrie through a Liebig Fellowship and a Ph.D. fellowship and by the TUM Junior Fellow Fund.

Author contributions

The authors contributed in the following manner: Conceptualization (S.Br. with inputs from P.C., P.D., J.M., E.J., Y.G., V.M., R.C., J.-B.I.), performed experiments (S.Br., P.D., J.M., P.R.A.Z., K.P., R.H., M.M., R.-F.S., J.-B.I. with inputs from P.C., S.M.H., E.J., O.B.-S., O.B.), conceptualized and designed small molecules synthesis (R.C., Y.G., V.M., V.B.-G., S.Ba., M.C.F.O. with inputs from D.L., P.R.), performed small molecules synthesis (D.L., P.R., C.B., M.V.B.), performed bioinformatics analysis (C.N., P.R.A.Z., S.M.H.), analyzed the data (S.Br., P.D., J.M., P.R.A.Z., S.M.H., P.C., E.J., Y.G., R.C.), wrote the paper (S.Br with inputs from S.M.H., E.J., Y.G., R.C., V.M., P.C., V.B.-G.).

Competing interests

A patent related to this work has been submitted.

References

1 Newman, D. J. & Cragg, G. M. Natural Products as Sources of New Drugs over the Nearly Four Decades from 01/1981 to 09/2019. *J Nat Prod* **83**, 770-803, doi:10.1021/acs.jnatprod.9b01285 (2020).

2 Bergmann, W. & Feeney, R. J. The isolation of a new thymine pentoside from sponges. *J Am Chem Soc* **72**, 2809-2810, doi:10.1021/ja01162a543 (1950).

3 Ellison, R. R. *et al.* Arabinosyl cytosine: a useful agent in the treatment of acute leukemia in adults. *Blood* **32**, 507-523 (1968).

4 Seo, Y., Cho, K. W., Rho, J.-R., Shin, J. & Sim, C. J. Petrocortynes and petrosiacetylenes, novel polyacetylenes from a sponge of the genus Petrosia. *Tetrahedron* **54**, 447-462, doi:10.1016/S0040-4020(97)10290-3 (1998).

5 Ortega, M. J., Zubía, E., Carballo, J. L. & Salvá, J. Fulvinol, a New Long-Chain Diacetylenic Metabolite from the Sponge Reniera fulva. *J Nat Prod* **59**, 1069-1071, doi:10.1021/np960436l (1996).

6 Gunasekera, S. P. & Faircloth, G. T. New acetylenic alcohols from the sponge Cribrochalina vasculum. *J Org Chem* **55**, 6223-6225, doi:10.1021/jo00312a035 (1990).

7 Zovko, A. *et al.* Marine sponge Cribrochalina vasculum compounds activate intrinsic apoptotic signaling and inhibit growth factor signaling cascades in non-small cell lung carcinoma. *Mol Cancer Ther* **13**, 2941-2954, doi:10.1158/1535-7163.MCT-14-0329 (2014).

8 El Arfaoui, D. *et al.* Identification of chiral alkenyl- and alkynylcarbinols as pharmacophores for potent cytotoxicity. *ChemMedChem* **8**, 1779-1786, doi:10.1002/cmdc.201300230 (2013).

9 Listunov, D. *et al.* Extended structural modulation of bio-inspired chiral lipidic alkynylcarbinols as antitumor pharmacophores. *Tetrahedron* **71**, 7920-7930, doi:10.1016/j.tet.2015.08.003 (2015).

10 Listunov, D. *et al.* From Natural to Artificial Antitumor Lipidic Alkynylcarbinols: Asymmetric Synthesis, Enzymatic Resolution, and Refined SARs. *Synthesis* **50**, 3114-3130, doi:10.1055/s-0037-1610006 (2018).

11 Carette, J. E. *et al.* Haploid genetic screens in human cells identify host factors used by pathogens. *Science* **326**, 1231-1235, doi:10.1126/science.1178955 (2009).

12 Wacker, S. A., Houghtaling, B. R., Elemento, O. & Kapoor, T. M. Using transcriptome sequencing to identify mechanisms of drug action and resistance. *Nat Chem Biol* **8**, 235-237, doi:10.1038/nchembio.779 (2012).

13 Bossaert, M. *et al.* Transcription-associated topoisomerase 2alpha activity is a major effector of cytotoxicity induced by G-quadruplex ligands. *eLife* **10**, doi:10.7554/eLife.65184 (2021).

14 Forment, J. V. *et al.* Genome-wide genetic screening with chemically mutagenized haploid embryonic stem cells. *Nat Chem Biol* **13**, 12-14, doi:10.1038/nchembio.2226 (2017).

15 Brockmann, M. *et al.* Genetic wiring maps of single-cell protein states reveal an off-switch for GPCR signalling. *Nature* **546**, 307-311, doi:10.1038/nature22376 (2017).

16 Brereton, P. *et al.* Pan1b (17betaHSD11)-enzymatic activity and distribution in the lung. *Mol Cell Endocrinol* **171**, 111-117, doi:10.1016/s0303-7207(00)00417-2 (2001).

17 Horiguchi, Y., Araki, M. & Motojima, K. Identification and characterization of the ER/lipid droplet-targeting sequence in 17beta-hydroxysteroid dehydrogenase type 11. *Arch Biochem Biophys* **479**, 121-130, doi:10.1016/j.abb.2008.08.020 (2008).

18 Filling, C. *et al.* Critical residues for structure and catalysis in short-chain dehydrogenases/reductases. *J Biol Chem* **277**, 25677-25684, doi:10.1074/jbc.M202160200 (2002).

19 Listunov, D. *et al.* Methinylogation Approach in Chiral Pharmacophore Design: from Alkynyl- to Allenyl-carbinol Warheads against Tumor Cells. *ChemMedChem* **13**, 1711-1722, doi:10.1002/cmdc.201800284 (2018).

20 Bourkhis, M. *et al.* Skeletal Optimization of Cytotoxic Lipidic Dialkynylcarbinols. *ChemMedChem* **13**, 1124-1130, doi:10.1002/cmdc.201800118 (2018).

21 Grant, C. V. *et al.* CRISPR-Cas9 Genome-Wide Knockout Screen Identifies Mechanism of Selective Activity of Dehydrofalcarinol in Mesenchymal Stem-like Triple-Negative Breast Cancer Cells. *J Nat Prod* **83**, 3080-3092, doi:10.1021/acs.jnatprod.0c00642 (2020).

22 Barretina, J. *et al.* The Cancer Cell Line Encyclopedia enables predictive modelling of anticancer drug sensitivity. *Nature* **483**, 603-607, doi:10.1038/nature11003 (2012).

23 Worch, J. C., Stubbs, C. J., Price, M. J. & Dove, A. P. Click Nucleophilic Conjugate Additions to Activated Alkynes: Exploring Thiol-yne, Amino-yne, and Hydroxyl-yne Reactions from (Bio)Organic to Polymer Chemistry. *Chem Rev* **121**, 6744-6776, doi:10.1021/acs.chemrev.0c01076 (2021).

24 Tornoe, C. W., Christensen, C. & Meldal, M. Peptidotriazoles on solid phase: [1,2,3]-triazoles by regiospecific copper(i)-catalyzed 1,3-dipolar cycloadditions of terminal alkynes to azides. *J Org Chem* **67**, 3057-3064, doi:10.1021/jo011148j (2002).

25 Rostovtsev, V. V., Green, L. G., Fokin, V. V. & Sharpless, K. B. A stepwise huisgen cycloaddition process: copper(I)-catalyzed regioselective "ligation" of azides and terminal alkynes. *Angew Chem Int Ed* **41**, 2596-2599, doi:10.1002/1521-3773(20020715)41:14<2596::AID-ANIE2596>3.0.CO;2-4 (2002).

26 Speers, A. E. & Cravatt, B. F. Profiling enzyme activities in vivo using click chemistry methods. *Chem Biol* **11**, 535-546, doi:10.1016/j.chembiol.2004.03.012 (2004).

27 Weerapana, E. *et al.* Quantitative reactivity profiling predicts functional cysteines in proteomes. *Nature* **468**, 790-795, doi:10.1038/nature09472 (2010).

28 Backus, K. M. *et al.* Proteome-wide covalent ligand discovery in native biological systems. *Nature* **534**, 570-574, doi:10.1038/nature18002 (2016).

29 Zanon, P. R. A., Lewald, L. & Hacker, S. M. Isotopically Labeled Desthiobiotin Azide (isoDTB) Tags Enable Global Profiling of the Bacterial Cysteinome. *Angew Chem Int Ed* **59**, 2829-2836, doi:10.1002/anie.201912075 (2020).

30 Zanon, P. R. A. *et al.* Profiling the Proteome-Wide Selectivity of Diverse Electrophiles. *ChemRxiv*, doi:10.33774/chemrxiv-2021-w7rss-v2 (2021).

31 Isom, D. G., Castaneda, C. A., Cannon, B. R. & Garcia-Moreno, B. Large shifts in pKa values of lysine residues buried inside a protein. *Proc Natl Acad Sci U S A* **108**, 5260-5265, doi:10.1073/pnas.1010750108 (2011).

32 Viedma-Poyatos, A. *et al.* Protein Lipoxidation: Basic Concepts and Emerging Roles. *Antioxidants (Basel)* **10**, doi:10.3390/antiox10020295 (2021).

33 Listunov, D. *et al.* Fluorophore-tagged pharmacophores for antitumor cytotoxicity: Modified chiral lipidic dialkynylcarbinols for cell imaging. *Bioorg Med Chem Lett* **25**, 4652-4656, doi:10.1016/j.bmcl.2015.08.029 (2015).

34 Vila, A. *et al.* Identification of protein targets of 4-hydroxynonenal using click chemistry for ex vivo biotinylation of azido and alkynyl derivatives. *Chem Res Toxicol* **21**, 432-444, doi:10.1021/tx700347w (2008).

35 Larrieu, D., Britton, S., Demir, M., Rodriguez, R. & Jackson, S. P. Chemical inhibition of NAT10 corrects defects of laminopathic cells. *Science* **344**, 527-532, doi:344/6183/527 [pii]

10.1126/science.1252651 (2014).
36 Blomen, V. A. *et al.* Gene essentiality and synthetic lethality in haploid human cells. *Science* **350**, 1092-1096, doi:10.1126/science.aac7557 (2015).
37 Shi, Y. *et al.* Rpn1 provides adjacent receptor sites for substrate binding and deubiquitination by the proteasome. *Science* **351**, doi:10.1126/science.aad9421 (2016).
38 Menendez-Benito, V., Verhoef, L. G., Masucci, M. G. & Dantuma, N. P. Endoplasmic reticulum stress compromises the ubiquitin-proteasome system. *Hum Mol Genet* **14**, 2787-2799, doi:10.1093/hmg/ddi312 (2005).
39 Mailand, N. *et al.* RNF8 ubiquitylates histones at DNA double-strand breaks and promotes assembly of repair proteins. *Cell* **131**, 887-900, doi:10.1016/j.cell.2007.09.040 (2007).
40 Preissler, S. & Ron, D. Early Events in the Endoplasmic Reticulum Unfolded Protein Response. *Cold Spring Harb Perspect Biol* **11**, doi:10.1101/cshperspect.a033894 (2019).
41 Kavanagh, K. L., Jornvall, H., Persson, B. & Oppermann, U. Medium- and short-chain dehydrogenase/reductase gene and protein families : the SDR superfamily: functional and structural diversity within a family of metabolic and regulatory enzymes. *Cell Mol Life Sci* **65**, 3895-3906, doi:10.1007/s00018-008-8588-y (2008).
42 Kedishvili, N. Y. *et al.* Evidence that the human gene for prostate short-chain dehydrogenase/reductase (PSDR1) encodes a novel retinal reductase (RalR1). *J Biol Chem* **277**, 28909-28915, doi:10.1074/jbc.M202588200 (2002).
43 Haeseleer, F. *et al.* Dual-substrate specificity short chain retinol dehydrogenases from the vertebrate retina. *J Biol Chem* **277**, 45537-45546, doi:10.1074/jbc.M208882200 (2002).
44 Tai, H. H., Cho, H., Tong, M. & Ding, Y. NAD+-linked 15-hydroxyprostaglandin dehydrogenase: structure and biological functions. *Current pharmaceutical design* **12**, 955-962, doi:10.2174/138161206776055958 (2006).
45 Cui, C. *et al.* Total Synthesis and Target Identification of the Curcusone Diterpenes. *J Am Chem Soc* **143**, 4379-4386, doi:10.1021/jacs.1c00557 (2021).
46 Shringarpure, R., Grune, T., Sitte, N. & Davies, K. J. 4-Hydroxynonenal-modified amyloid-beta peptide inhibits the proteasome: possible importance in Alzheimer's disease. *Cell Mol Life Sci* **57**, 1802-1809, doi:10.1007/pl00000660 (2000).
47 Bray, J. E., Marsden, B. D. & Oppermann, U. The human short-chain dehydrogenase/reductase (SDR) superfamily: a bioinformatics summary. *Chemico-biological interactions* **178**, 99-109, doi:10.1016/j.cbi.2008.10.058 (2009).
48 Chang, K. H. *et al.* A gain-of-function mutation in DHT synthesis in castration-resistant prostate cancer. *Cell* **154**, 1074-1084, doi:10.1016/j.cell.2013.07.029 (2013).
49 Thomas, L. & Sharifi, N. Germline HSD3B1 Genetics and Prostate Cancer Outcomes. *Urology* **145**, 13-21, doi:10.1016/j.urology.2020.08.028 (2020).
50 Hearn, J. W. D. *et al.* HSD3B1 Genotype and Clinical Outcomes in Metastatic Castration-Sensitive Prostate Cancer. *JAMA Oncol* **6**, e196496, doi:10.1001/jamaoncol.2019.6496 (2020).
51 Kallberg, Y., Oppermann, U. & Persson, B. Classification of the short-chain dehydrogenase/reductase superfamily using hidden Markov models. *FEBS J* **277**, 2375-2386, doi:10.1111/j.1742-4658.2010.07656.x (2010).
52 Hacker, S. M. *et al.* Global profiling of lysine reactivity and ligandability in the human proteome. *Nat Chem* **9**, 1181-1190, doi:10.1038/nchem.2826 (2017).
53 Abbasov, M. E. *et al.* A proteome-wide atlas of lysine-reactive chemistry. *Nat Chem*, doi:10.1038/s41557-021-00765-4 (2021).
54 Costantini, L. M. *et al.* A palette of fluorescent proteins optimized for diverse cellular environments. *Nat Commun* **6**, 7670, doi:10.1038/ncomms8670 (2015).

55 Olenych, S. G., Claxton, N. S., Ottenberg, G. K. & Davidson, M. W. The fluorescent protein color palette. *Curr Protoc Cell Biol* **Chapter 21**, Unit 21 25, doi:10.1002/0471143030.cb2105s36 (2007).

56 Britton, S. *et al.* DNA damage triggers SAF-A and RNA biogenesis factors exclusion from chromatin coupled to R-loops removal. *Nucleic Acids Res* **42**, 9047-9062, doi:10.1093/nar/gku601 (2014).

57 Britton, S., Coates, J. & Jackson, S. P. A new method for high-resolution imaging of Ku foci to decipher mechanisms of DNA double-strand break repair. *J Cell Biol* **202**, 579-595, doi:10.1083/jcb.201303073 (2013).

58 Carette, J. E. *et al.* Ebola virus entry requires the cholesterol transporter Niemann-Pick C1. *Nature* **477**, 340-343, doi:10.1038/nature10348 (2011).

59 Slaymaker, I. M. *et al.* Rationally engineered Cas9 nucleases with improved specificity. *Science* **351**, 84-88, doi:10.1126/science.aad5227 (2016).

60 Streit, M. *et al.* Ordino: a visual cancer analysis tool for ranking and exploring genes, cell lines and tissue samples. *Bioinformatics* **35**, 3140-3142, doi:10.1093/bioinformatics/btz009 (2019).

61 Mariette, J. *et al.* NG6: Integrated next generation sequencing storage and processing environment. *BMC Genomics* **13**, 462, doi:10.1186/1471-2164-13-462 (2012).

62 Li, H. & Durbin, R. Fast and accurate short read alignment with Burrows-Wheeler transform. *Bioinformatics* **25**, 1754-1760, doi:10.1093/bioinformatics/btp324 (2009).

63 Dobin, A. *et al.* STAR: ultrafast universal RNA-seq aligner. *Bioinformatics* **29**, 15-21, doi:10.1093/bioinformatics/bts635 (2013).

64 Liao, Y., Smyth, G. K. & Shi, W. featureCounts: an efficient general purpose program for assigning sequence reads to genomic features. *Bioinformatics* **30**, 923-930, doi:10.1093/bioinformatics/btt656 (2014).

65 McKenna, A. *et al.* The Genome Analysis Toolkit: a MapReduce framework for analyzing next-generation DNA sequencing data. *Genome Res* **20**, 1297-1303, doi:10.1101/gr.107524.110 (2010).

66 Cingolani, P. *et al.* A program for annotating and predicting the effects of single nucleotide polymorphisms, SnpEff: SNPs in the genome of Drosophila melanogaster strain w1118; iso-2; iso-3. *Fly (Austin)* **6**, 80-92, doi:10.4161/fly.19695 (2012).

67 Shannon, P. *et al.* Cytoscape: a software environment for integrated models of biomolecular interaction networks. *Genome Res* **13**, 2498-2504, doi:10.1101/gr.1239303 (2003).

68 Perez-Riverol, Y. *et al.* The PRIDE database and related tools and resources in 2019: improving support for quantification data. *Nucleic Acids Res* **47**, D442-D450, doi:10.1093/nar/gky1106 (2019).

69 Thomsen, M. C. & Nielsen, M. Seq2Logo: a method for construction and visualization of amino acid binding motifs and sequence profiles including sequence weighting, pseudo counts and two-sided representation of amino acid enrichment and depletion. *Nucleic Acids Res* **40**, W281-287, doi:10.1093/nar/gks469 (2012).

70 Rozie, A. *et al.* Alkyne-Tagged Analogue of Jaspine B: New Tool for Identifying Jaspine B Mode of Action. *Chembiochem* **19**, 2438-2442, doi:10.1002/cbic.201800496 (2018).

1052 **FIGURES & FIGURE LEGENDS**

Figure 1

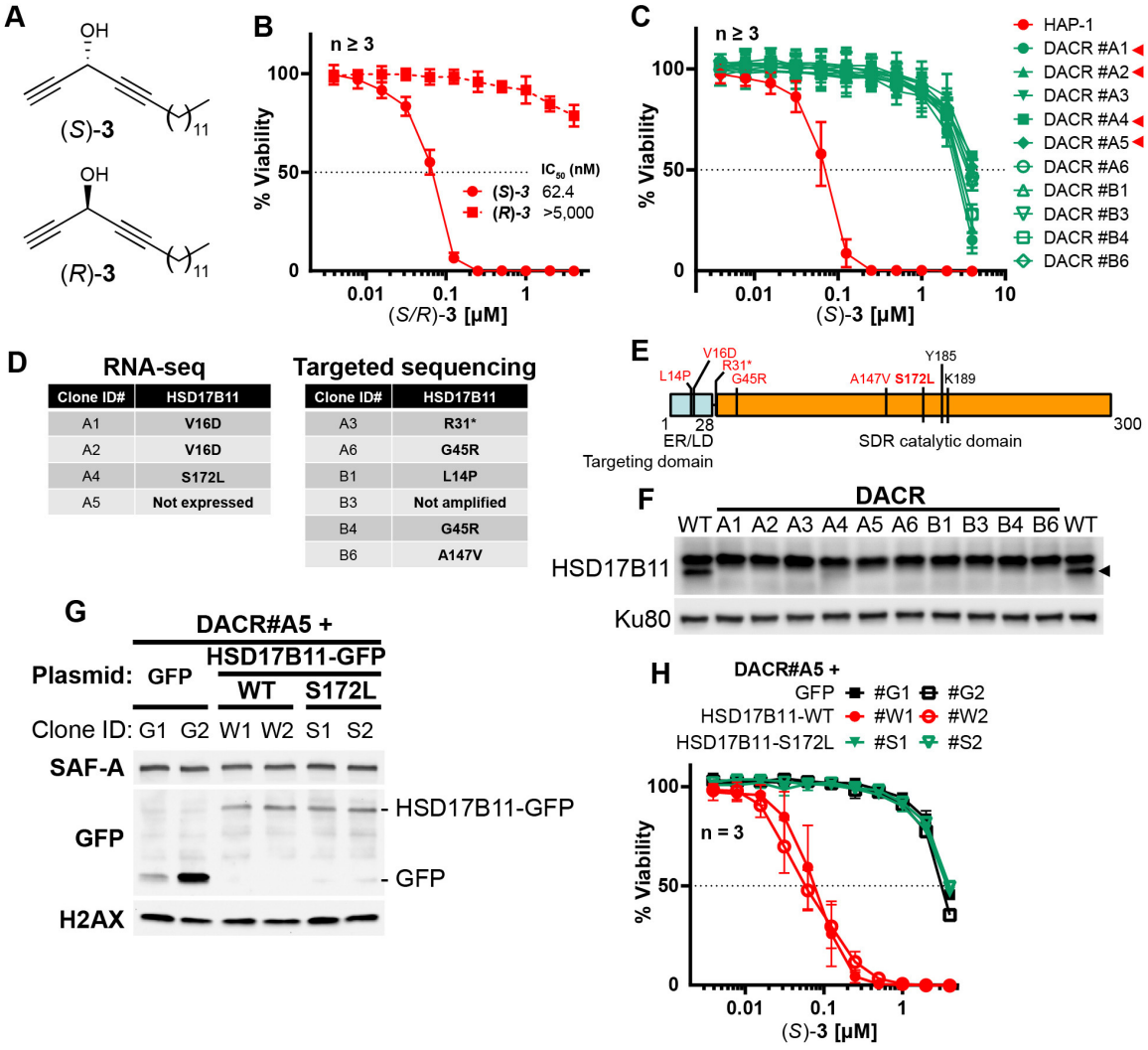

Clone ID#	HSD17B11
A1	V16D
A2	V16D
A4	S172L
A5	Not expressed

Clone ID#	HSD17B11
A3	R31*
A6	G45R
B1	L14P
B3	Not amplified
B4	G45R
B6	A147V

1053

Figure 1: HSD17B11 is necessary for DAC (*S*)-3 cytotoxic activity. A. DAC (*S*)-**3** and (*R*)-**3** structures. **B.** Cell viability analysis of HAP-1 or U2OS cells treated for 72 h with the indicated concentrations of (*S*)- or (*R*)-**3**. **C.** Cell viability analysis of individual DAC-resistant clones or wild-type HAP-1 treated for 72 h with the indicated concentrations of (*S*)-**3**. **D.** List of mutations identified by RNA-seq or targeted sequencing of HSD17B11 in individual DAC-resistant clones. **E.** Schematic representation of HSD17B11 functional domains. The positions of the identified mutations are indicated in red. The Y185, K189 (indicated in black) and S172 amino acids are critical for catalysis. **F.** Analysis by immunoblotting of HSD17B11 levels in wild-type HAP-1 and DAC-resistant clones. Ku80 was used as a loading control. The black arrow indicates HSD17B11 position. **G.** Analysis by immunoblotting of HSD17B11-GFP levels in individual clones of DAC-resistant clone A5 complemented with GFP, wild-type or S172L mutant HSD17B11-GFP. SAF-A and total H2AX were used as loading controls. **H.** Cell viability analysis of individual clones of DAC-resistant clone A5 complemented with GFP, wild-type or S172L mutant HSD17B11-GFP treated for 72 h with the indicated concentrations of (*S*)-**3**.

Figure 2

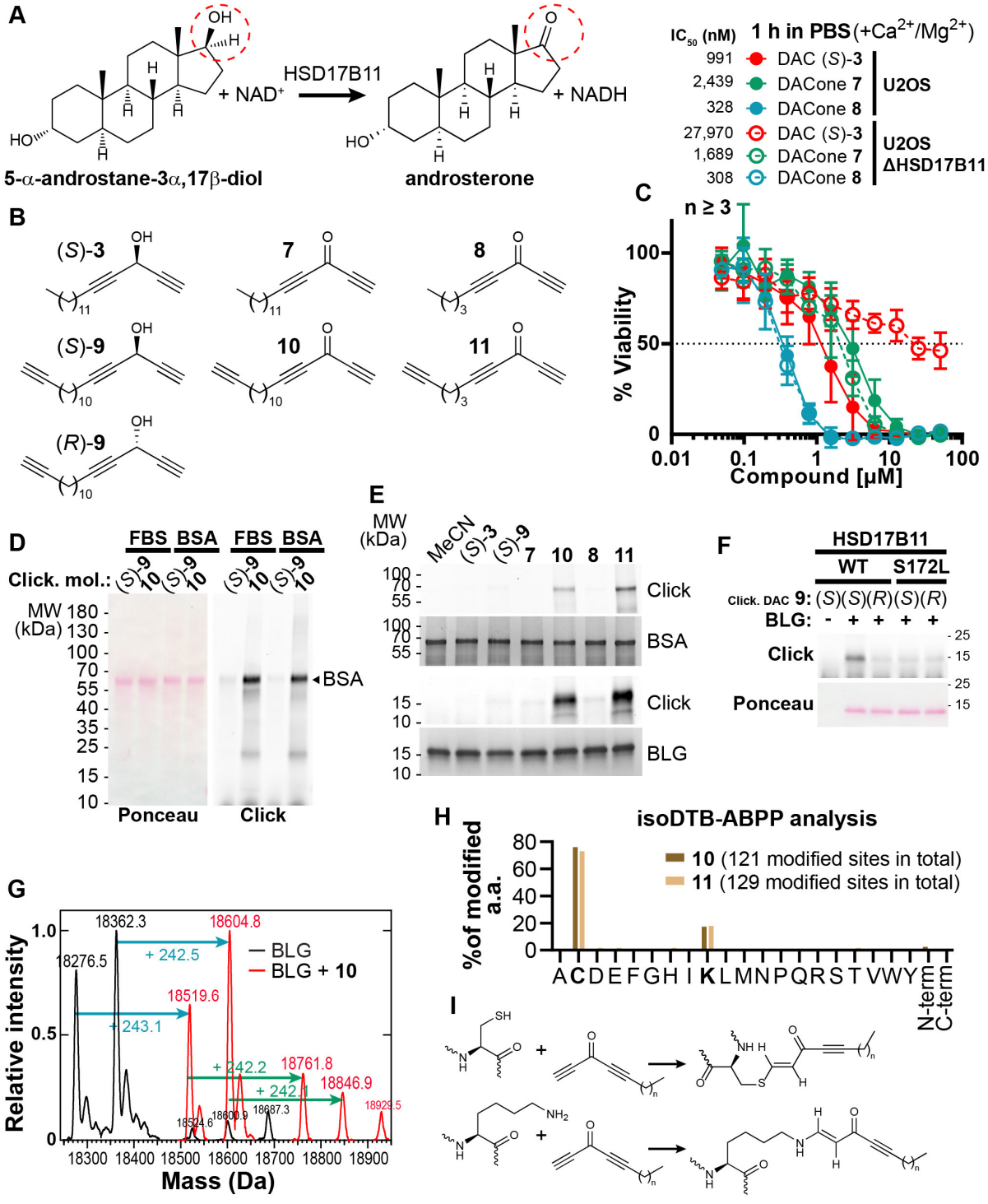

Figure 2: DACones are protein reactive species. A. Reaction catalyzed by HSD17B11. **B.** Clickable DACs and DACones used in the study. **C.** Viability analysis of U2OS cells treated in PBS for 1 h with (*S*)-**3** or DACones and incubated for an additional 72 h after drug washout. **D.** FBS or purified BSA were incubated 40 min at 30 °C with clickable DAC (*S*)-**9** or clickable DACone **10**. After reaction, CuAAC was used to ligate an azido-AlexaFluor647 to clickable molecules. Modified proteins were detected by scanning membrane fluorescence after SDS-PAGE and transfer. Ponceau S stains total proteins. **E.** BSA or BLG were incubated with the indicated DACs or DACones, as in **D**. After reaction, modified proteins were detected as in **D**. Coomassie stains total proteins. **F.** WT or S172L HSD17B11-GFP were immunoprecipitated from complemented U2OS KO HSD17B11 cells and incubated with clickable DAC **9** and BLG. After reaction modified proteins were detected as in **d**. **G.** Analysis by direct-infusion mass spectrometry of purified BLG (mixture of isoform A and B) modified or not by DACone **10**. Cyan and green arrows indicate the formation of a first and second adduct, respectively. **H.** % of each amino acid detected as modified by DACones **10** or **11** in U2OS extracts as determined using a isoDTB-ABPP-based framework. **I.** Proposed reactions of DACones with cysteine and lysine side chains in proteins.

Figure 3

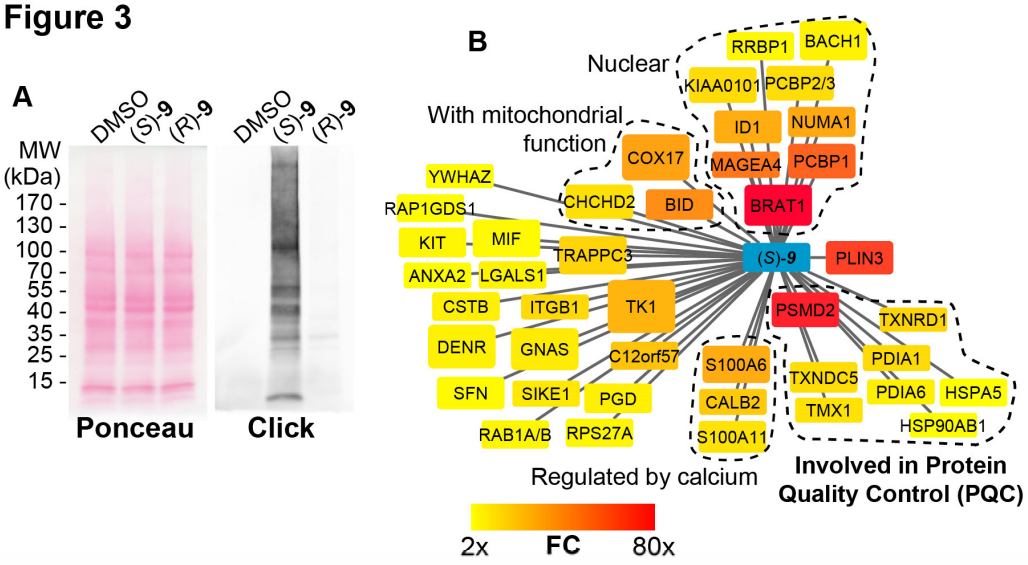

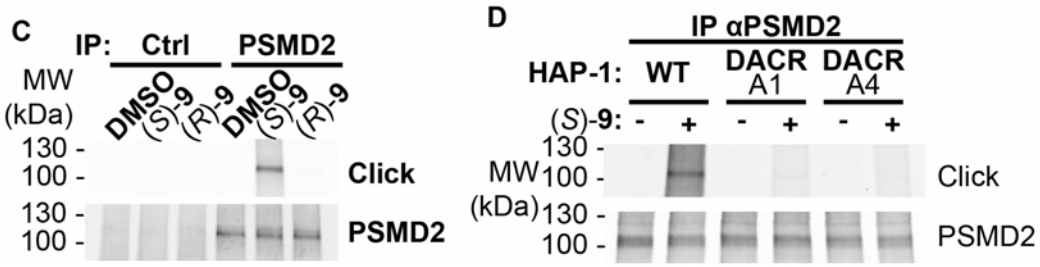

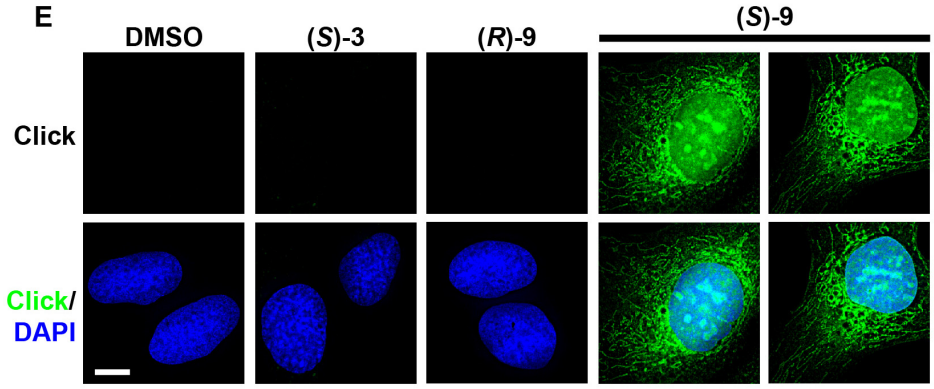

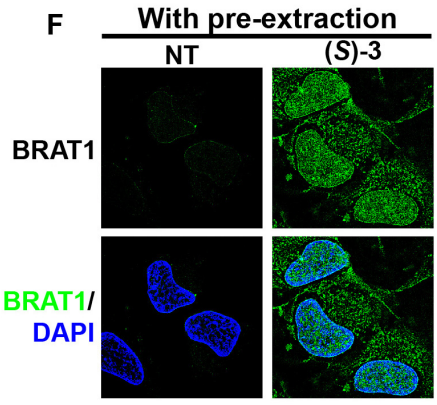

1086

Figure 3: (*S*)-**DACs lipoxidize multiple cellular proteins, triggering their association with cellular membranes. A.** U2OS cells were incubated for 2 h with 2 µM (*S*)- or (*R*)-**9**, proteins were extracted and DAC-modified proteins were detected by CuAAC-mediated ligation of azido-AlexaFluor-647 to clickable molecules, separation by SDS-PAGE, transfer to a membrane which was scanned for fluorescence. **B.** Landscape of proteins modified in U2OS cells by clickable DAC (*S*)-**9** computed from 3 independent experiments. Fold enrichment (FC) as compared to the clickable (*R*)-**9** is computed and color-coded as depicted. Box size corresponds to -log(p) computed as described in the materials and methods section. **C.** PSMD2 or control immunoprecipitations (Ctrl) were performed from extracts of U2OS cells treated 2 h with 2 µM clickable DAC (*S*)- or (*R*)-**9**. DAC-modified proteins were detected by CuAAC-mediated ligation of azido-AlexaFluor-647 to clickable molecules, separation by SDS-PAGE, transfer to a membrane, which was scanned for fluorescence. PSMD2 was subsequently visualized by immunoblotting. **D.** PSMD2 immunoprecipitations were performed from extracts of wild-type or DAC-resistant HAP-1 cells treated or not for 2 h with 2 µM clickable DAC (*S*)-**9**. DAC-modified proteins were detected by CuAAC-mediated ligation as in (c) PSMD2 was subsequently visualized by immunoblotting. **E.** U2OS cells were treated 2 h with 0.5 µM DAC, fixed, permeabilized, and clickable molecules were detected by click with AlexaFluor488 azide. **F.** U2OS expressing GFP-BRAT1 were treated 2 h with 1 µM (*S*)-**3**, pre-extracted, fixed and processed for analysis by fluorescence microscopy.

Figure 4

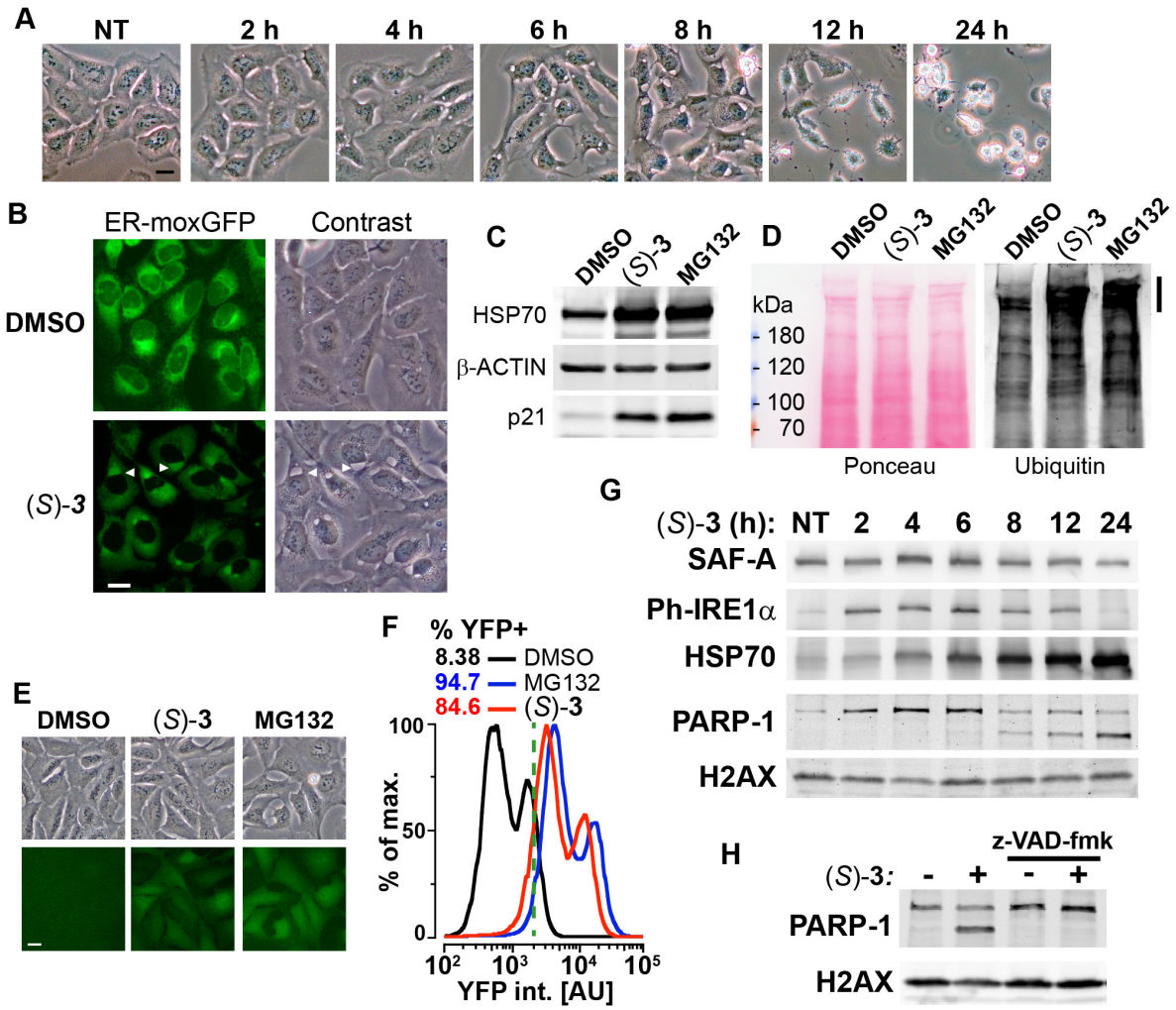

1106

Figure 4: DAC (*S*)-3 triggers ER-stress, proteasome inhibition and apoptosis. A. U2OS stably co-expressing a GFP variant addressed and retained in the endoplasmic reticulum were treated with 1 µM (*S*)-**3** and monitored by live imaging. Representative pictures of U2OS cells either untreated (NT) or treated with 1 µM (*S*)-**3** for the indicated time. **B.** Representative pictures of U2OS with stably GFP-labeled endoplasmic reticulum and either untreated or treated for 8 h with 1 µM (*S*)-**3**. **C.** Immunoblotting of extracts from U2OS untreated or treated with 1 µM (*S*)-**3** or 20 µM MG132 for 8 h. **D.** Immunoblotting of ubiquitin in extracts from U2OS untreated or treated with 1 µM (*S*)-**3** or 20 µM MG132 for 2 h. High molecular weight ubiquitin conjugates are indicated by a vertical bar on the right. **E.** Representative pictures of U2OS stably expressing Ub-G76V-YFP and either untreated or treated for 4 h with 1 µM (*S*)-**3** or 20 µM MG132. **F.** Analysis of YFP fluorescence by flow cytometry of U2OS Ub-G76V-YFP treated as described in **E.** % of cells scored as positives using the vertical green bar as a threshold are indicated. **G.** Immunoblotting using extracts from U2OS cells treated with 1 µM (*S*)-**3** for increasing times, indicated in hours. **H.** Immunoblotting using extracts from U2OS cells treated with 1 µM (*S*)-**3** for 12 h with or without 50 µM z-VAD-fmk.

Figure 5

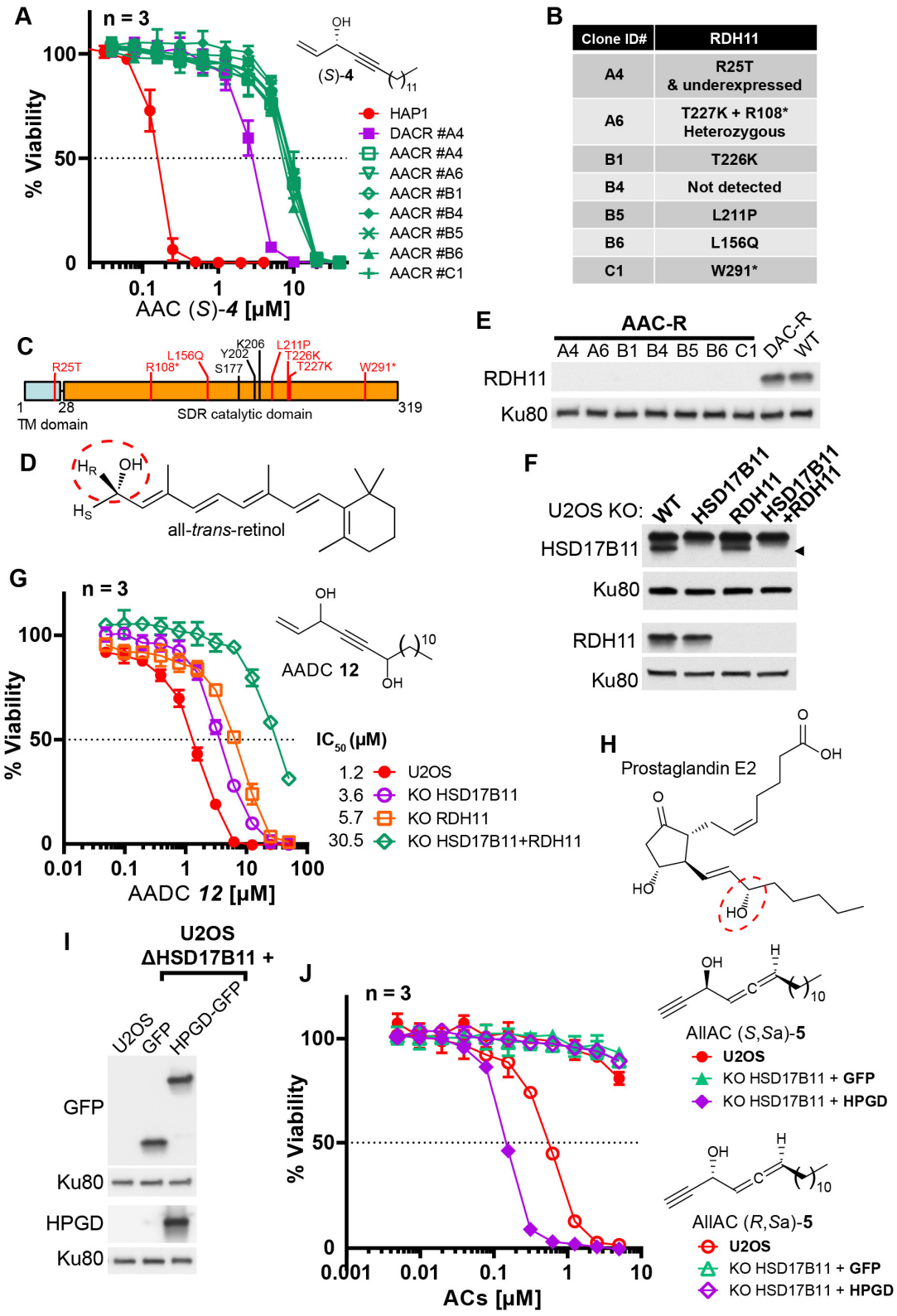

1123

Figure 5: Bioactivation of other lipidic alkynylcarbinols by specific SDRs. A. Cell viability analysis of wild-type HAP-1, DACR clone A4 and AACR clones treated with AAC (*S*)-**4**. **B.** List of mutations identified on RDH11 by RNA-seq of individual AACR clones. **C.** Schematic representation of RDH11 with, in red, the positions of the mutations identified and, in black, the three amino acids critical for catalysis. TM = single-pass transmembrane domain. **D.** Structure of all-*trans*-retinol, a substrate for RDH11. **E.** Analysis by immunoblotting of RDH11 levels in wild-type HAP-1, in DACR clone A4 and in the different AACR clones. **F.** Analysis by immunoblotting of RDH11 and HSD17B11 levels in wild-type U2OS or clones inactivated for either HSD17B11, RDH11 or both. **G.** Cell viability analysis of wild-type U2OS or U2OS clones inactivated for HSD17B11, RDH11, or both and treated with AADC **12**. **H.** Structure of prostaglandin E2, a substrate of HPGD. **I.** Analysis by immunoblotting of GFP and HPGD levels in WT U2OS or U2OS KO HSD17B11 stably complemented with GFP or HPGD-GFP. **J.** Cell viability analysis of U2OS or U2OS inactivated for HSD17B11, stably complemented with either HSD17B11-GFP or HPGD-GFP and treated for 72 h with AllAC (*S,Sa*)- or (*R,Sa*)-**5**.

Figure 6

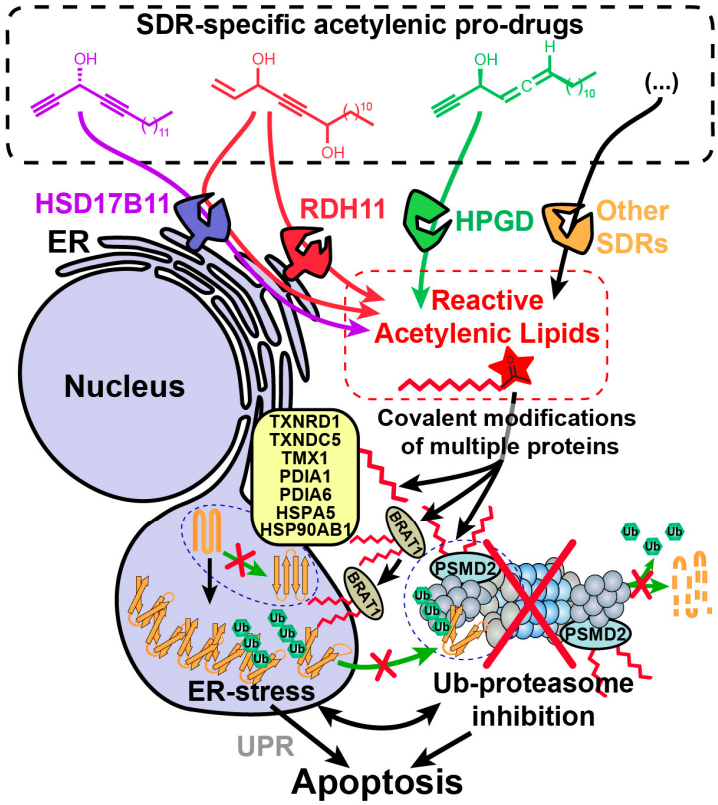

Figure 6: Model depicting the stereospecific bioactivation of alkynylcarbinol-containing compounds by specific SDRs into cytotoxic protein-reactive species. The protein reactive species generated upon bioactivation modify several proteins including the essential 26S proteasome subunit PSMD2, thereby triggering Ub-proteasome system (UPS) inhibition, ER-stress, activation of the Unfolded Protein Response (UPR) and cell death mediated by apoptosis.

Graphical abstract